Fys - 3931
Master's Thesis in Space Physics

Analysis of the dynamical behavior of the Minidusty rocket payloads, and its influence on the plasma probe measurements

María Nácher Rodríguez

June, 2007

Faculty of Science
Department of Physics and Technology

University of Tromsø

Fys - 3931
Master's Thesis in Space Physics

Analysis of the dynamical behavior of the Minidusty rocket payloads, and its influence on the plasma probe measurements

María Nácher Rodríguez

June, 2007

It's time to face reality my friends ...
We're not exactly rocket scientists
Gary Larson's The far side

Acknowledgements

First of all I would like to thank Professor Ove Havnes, for sharing with me his knowledge about a world that was new for me, the world of sounding rockets. He has been patient with me and I know how difficult it is to teach a person almost from the beginning in a new field.

I also want to thank Sveinung Olsen, for all his help. Maybe you think it was not that much, but it was what I needed. The pictures were great!!

Muchas gracias muchita, se que vas a leer ésto y te va a hacer ilusión. Gracias por animarme y esperar hasta que 'la partícula' llegara al suelo. También me hace ilusón dar las gracias a la gente que, aunque no vaya a leer este trabajo, me ha dicho todos los días que me iba a dar tiempo a acabarlo; Mini, Bino, Cris, San, Nati, Raquel, Giulio,... Muchas gracias a tí también papá, por llamarme cada vez que ceno fruta (ahora ya no me sorprende, simplemente espero la llamada) e intentar convencerme de que le llorara a mi supervisor, jejeje.

A estas alturas, 25 de Junio, te he dado tantas veces las gracias Enrique que he decidido no dártelas más hasta que me cuides mientras duerma maana en el aeropuerto. Está bien, me retracto, gracias por ser la persona más buena del mundo, y además estar conmigo! Ha sido un ao delicioso junto al mundo de los cohetes y las auroras...

Contents

List of Figures

Chapter 1

Introduction

The Earth is a planet with atmosphere. There is a long history about how people measured and interpreted the signs of our atmosphere, but there is also a longer history about the evolution of the atmosphere itself.

During the five billion years of the Earth's history, the atmosphere has suffered plenty of permutations until reaching the actual status. For the first 500 million years it was mainly formed of hydrogen, water vapor, methane, and carbon dioxide. Afterwards it changed to CO_2, CO, H_2O, N_2, and H_2. The oceans were formed four billion years ago, due to the condensation of this water vapor. However, life was not possible due to the absence of free oxygen. It was not until one million years ago that organisms called blue-green algae used the energy from the sun to split molecules of H_2O and CO_2, and recombined them into organic compounds and molecular oxygen O_2, starting that way the process that would transform the atmosphere in the one we know today [1].

From the ancient times people have observed and studied the atmosphere mainly to reach a more accurate weather forecast, and until the year 1643 these studies consisted basically of simple observations. Afterwards, new technology was introduced, like the barometer, invented by Torricelli, followed by the hygrometer in 1644. From that moment on, atmospheric instrumentation became more and more sophisticated thanks to people like Daniel Fahrenheit or Laurent Lavoisier [2]. With the development of humanity and their instrumentation, new theories and scientists started to be more interested in other characteristics of the atmosphere. For example Kristian Birkeland tried to explain the phenomena happening above 100 km, like the northern lights, at the beginning of the 20th century [3].

A more detailed study of the atmosphere, besides the meteorological phenomena, was possible due to the use of balloons carrying radiosondes, rockets and even satellites. With the help of such rockets, as the ones described in

this report, it is possible to take measurements and explain phenomena occurring at ∼85 km, like the noctilucent clouds and the polar mesospheric summer echoes.

1.1 Earth's Atmosphere

The planet Earth possesses a magnetic field. This magnetic field can be approximated, at the Earth's surface, by a magnetic dipole placed at the Earth's center and tilted around 11° [4]. The gases flowing around the Earth are retained by the Earth's gravity, due to its magnetic field. This layer of gases is called atmosphere. The air consists mainly of nitrogen N_2 and oxygen O_2, although other gases can be found too. In dry air at sea level, the composition is as follows: 78.03% nitrogen, 20.99% oxygen, 0.94% argon, 0.03% carbon dioxide, and 0.0017% other gases [5].

1.1.1 Layers

The atmosphere absorbs ultraviolet solar radiation, protecting life on Earth. It also reduces the temperature extremes between day and night. However, the temperature profile and composition of air along the atmosphere is not constant. We can differentiate five distinct layers using the temperature profile, chemical composition, movement, and density; although the temperature distribution is the main characteristic [1]. This layers are presented in Figure 1.1.

The temperature falls with height in the lowest layer, called troposphere, with a ratio of 6.5 K/km. The troposphere begins at the surface and extends to 8 km, at the poles, and 16 km, at the equator. The first broken line represents the tropopause, which separates the troposphere and the stratosphere. Together, the troposphere and the tropopause are called the lower atmosphere. The stratosphere begins just after the tropopause and extends to ∼50 km. Inside of it, is located the ozone layer at ∼30 km. This layer has a high concentration of ozone O_3, which produces a high absorption of certain components of the ultraviolet light from the sun, and therefore increases the temperature at those heights. The stratopause separates the stratosphere and the mesosphere, where the temperature falls again. The mesosphere starts in the stratopause and extends to 85 km, where the mesopause is located. The stratosphere and mesosphere are called the middle atmosphere. Above 85 km we find the thermosphere, which extends to 600 km, and is referred as the upper atmosphere. Here the temperature increases again with height and it is well known until 100 km, but then the uncertainty about the tem-

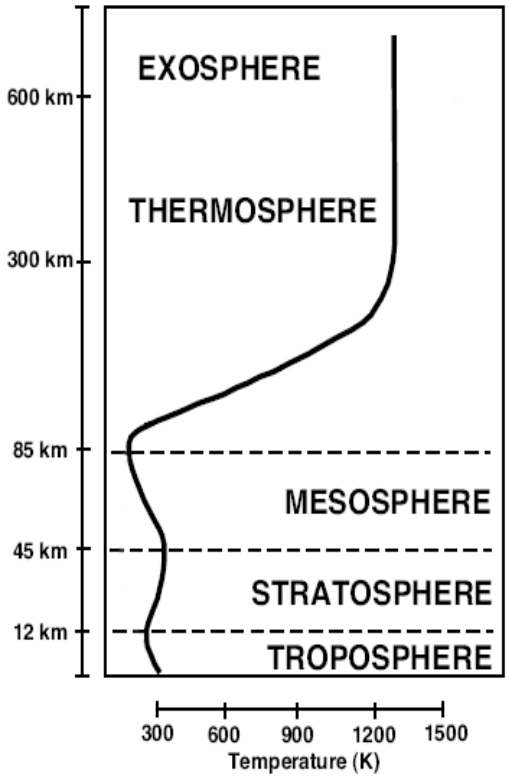

Figure 1.1: Temperature profile in the atmosphere. Credit: [6]

perature increases. Inside the thermosphere, we find a layer of atoms, which are ionized by solar radiation. This is the ionosphere, and here is where the phenomenon Aurora Borealis takes place. The exosphere is above 600 km, where the temperature remains uniform. There is no well defined boundary between the exosphere and the outer space; the atmosphere becomes thinner and thinner and finally it fades into space [1], [6].

1.1.2 Phenomena in the upper mesosphere

The coldest place in the Earth's atmosphere is the mesopause, ∼88 km. The temperature here changes depending on the season, as we can see in Figure 1.2. During winter the temperature is usually above 200° K, whereas in summer it drops even below 100° K [7]. These low temperatures allow the water vapor in the mesopause to become ice particles between 80 km and 90 km [8].

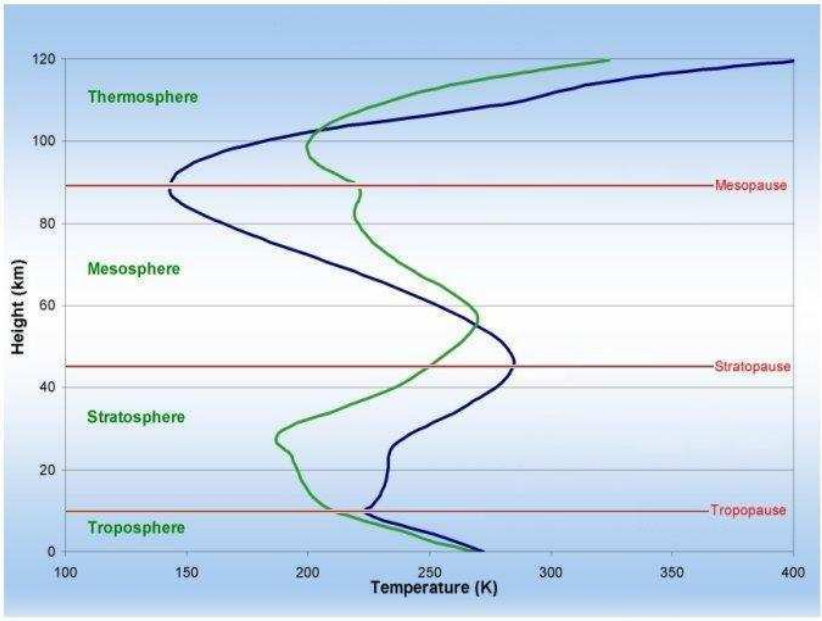

Figure 1.2: Atmospheric temperature above Davis station, Antarctica, in January (blue) and July (green). Credit: [9]

During summer, when the temperatures are so low, some interesting phenomena occur in the highest part of the mesosphere. The ice particles cited before are responsible of the formation of noctilucent clouds (NLC), also called polar mesospheric clouds (PMC). These clouds consist of nonspherical particles which have grown so much that scatter light, which is visible from ground and satellites. Their typical size is between 50 nm and 100 nm [10]. NLC can be seen when the sun is shining on them and not on the lower atmosphere, which means the sun should be below the horizon.

This is not the only phenomena that takes places in the upper mesosphere in summer. The smaller particles can become highly charged if they are contaminated by materials such as metals [7]. Then, transported by the turbulent velocity field, that is present in that region, they produce irregularities in the radio refractive index [8], which can be noticed as a strong radar backscatter (echoes) at frequencies from 50 MHz to 1.3 GHz [7]. This phenomenon is called polar mesospheric summer echoes (PMSE).

It has also been observed that an overshoot effect in the backscattered power is produced when heating these charged particles. This effect is due to smoother variations in the electron density gradients, produced by the high ascent in the temperature, and it is followed by the re-establishment of the

irregularities in the electron density when turning off the heater [11].

1.1.3 Instrumentation

For studying all these and other effects some ground-based instruments like radars, lidars, ionosondes, sensors, and radiometers can help us. Also satellites are used for these purposes. Unfortunately the best resolution of all these ground instruments is around 100-200 m, not good enough when the region being investigated is 10 km. Apart from this instrumentation we should consider balloons and rockets, because they can carry instruments into the regions of the middle and upper atmosphere.

Although the rocket was invented before the balloon, by the Chinese around the 13^{th} century, was in fact the balloon the first to be used for research of the atmosphere. The balloon was invented at the end of the 18^{th} century, and it has many advantages in its use for high altitude research. On the one hand it is lighter than air, and it does not require energy to keep flying, but on the other hand the instrumentation carried should be very light to reach high altitudes. The latter is one of the reasons why nowadays the balloon is used in combination with other instruments, such as sounding rockets [5].

The term *sounding rocket* comes from the nautical term 'to sound', i.e. to take measurements. They carry the necessary instrumentation for achieving the scientific goals, and also devices for checking and making them work, such as batteries, called the housekeeping of the rocket. The greatest advantage they provide is to take in situ measurements with a really good height resolution (a few times 0.10 m), which depends directly on the frequency of sending data. These data is sent to Earth by telemetry links, which transfer the data from the payload directly to telemetry stations on the ground [12]. On the other hand ground-based instruments are always working, whereas for taking measurements in situ you need to build the rocket, build the payload, prepare the launch, launch it and only if it works properly, you will have the data. With rockets the process is rougher, slower, and sometimes unprofitable.

There is also another reason for the necessity of sounding rockets. There are some measurements that can not be taken with radars or lidars, like turbulence, and rockets can measure them. The 80-90 km altitude range is the region in the atmosphere where gravity waves propagating from below grow unstable and produce turbulence. This turbulence is the cause of the formation of structures by the dust particles and hence of PMSE, so it's very important to be able to measure it [8].

Due to the hard work required to launch a rocket, it is better to launch it

when interesting measurements can be assured. Then, an idea rises: to use ground-based instruments and sounding rockets together. The combination of both is perfect for investigating the PMSE for example, because with radars you can detect the presence of these strong echoes and then with the rocket being launched in these conditions, the measurements taken will be the interesting ones. It is also of interest the state of the particles when no PMSE are detected, so here also the instrumentation on ground makes its part, assuring that no PMSE is observed. Although the appropriate would be to have both facilities near, ground instrumentation and rocket range, sometimes it is impossible.

In Norway these places are not so far. Andøya Rocket Range (ARR) is located in Andenes (69º17' N and 16º01' E) [13], and it is a optimum place for launching sounding rockets because of its position next to the ocean. The ground-based instruments used in conjunction with ARR are located in ALOMAR also located in Andenes (69º16'42" N and 16º00'31" E, 380 m altitude) [14], EISCAT Tromsø (69º35'11" N and 19º13'38" E, 86.28 m altitude) [15], and EISCAT Longyearbyen (78º09'11" N and 16º01'44" E, 445 m altitude) [15]. Combining these facilities, the probability of success in a launch campaign increases.

1.2 Sounding rockets

Sounding rockets are powerful instruments for measuring phenomena occurring up in the atmosphere. They fly through the areas of interest, and appropriate instrumentation are placed inside to take the desired measurements.

1.2.1 Main structure

The rocket structure comprises the shroud of the rocket. It is divided into the booster, the front end, also called the dart, and the interstage, also called radax joint or radial-axial joint, which is an interface to join the booster and the dart [16].

When starting a scientific project with sounding rockets, the aspects to consider for choosing the correct rocket are: the booster, the dart, and the propellant [16]. The booster design comprises the design of the fins, lugs and interstage. The design of the interstage depends on the dart and booster chosen, because it is going to join two pieces with different diameters. The design of the lugs depends on the structure from where the rocket is going to be launched. The dart performance depends on the ballistic coefficient of the body. In some instances a heavier dart will travel higher of farther

than a lighter one. The optimized performance of the dart is dependent on, at least, the launcher elevation and weight of the dart. Therefore a slight payload weight variation will alter the total performance capability and resulting experimental time. Also, variations in the total dart weight will change the dart velocity at burnout, resulting in a different thermal profile, which we should consider in the design of the thermal protection. The selection of dart will also depend on the payload and its mission. For choosing the proper booster and dart we should look at the 'spider plot'. Here we will find the distances the rocket can reach both in altitude and in range dependent on the dart weight and the elevation of the launcher. The propellant used commonly in sounding rockets is solid propellant. For choosing between propellants we will take a look at the curve of thrust versus time, which indicates also the burnout time, and also at the total impulse [16].

1.2.2 Basic principle

The principle why a rocket flies is simple, gases are ejected at high velocity from a combustion chamber. In accelerating the gases to high velocities the chamber experiences a force, which is the result of the third Newton's law of motion: to every action there is an equal and opposite reaction. The thrust on the rocket is equal to the rate of fuel consumption times the exhaust velocity [5].

1.2.3 Flight

The flight of the sounding rockets is always a ballistic flight, like an arrow, and it follows the parabola in one of the edges of an ellipse with one of the focus on the Earth's center. There is no possibility of changing the trajectory once it is launched. The rocket leaves the ground with the appropriate elevation and azimuth angles and follows an almost linear trajectory until it reaches the burnout, i.e. moment when the propellant is totally consumed. The booster motor imparts energy into the dart to provide the velocity required to continue the intended trajectory and allow mission fulfilment [16]. Around the burnout, the booster motor separates from the payload, due to the differential drag of the two bodies, leaving the payload continue the flight alone.

When the rocket arrives to the apogee its position is not horizontal, but the nosecone is still looking to space. Therefore we need that the altitude reached by the rocket is sufficient high, to give the rocket enough time to turn its nosecone before reaching the area of interest. This is wanted in

order to take measurements again during the second part of the flight, when it is returning to ground.

During the flight four forces act on a rocket: the weight, the thrust, the lift, and the drag [17]. The weight is the field force generated by the Earth's gravitational attraction on the rocket. It directly depends on the mass of the rocket, and it is directed towards the center of the Earth starting in the center of gravity of the rocket. The thrust is the mechanical force, which moves the rocket, generated by the propulsion system following Newton's third law of motion. The direction is normally along the longitudinal axis of the rocket through its center of gravity, and the magnitude depends on the ratio of fuel consumption and the exhaust velocity. The other two forces, lift and drag, are aerodynamic forces. They depend on some performances of the rocket, such as shape, size, velocity, but also on properties of the air the rocket flies through. They are mechanical forces because they are generated by the difference in velocity between the rocket and the air. Both, lift and drag, start in the center of pressure of the rocket, but whereas drag is opposed to the direction of motion, lift acts perpendicular to it.

The center of gravity should not be confused with the center of pressure. The center of gravity of the rocket, also called the center of mass, is the point where the rocket's mass behaves as if it was concentrated in that point. Said in other words, is the average location of the rocket's weight [17]. Whereas in the center of gravity the weight is evenly distributed, in the center of pressure are the aerodynamic forces the ones evenly distributed. The center of pressure must be a minimum of one body diameter behind the center of gravity on a rocket to ensure stability.

1.2.4 Motion during flight

The stability is one of the most important things that determine the success of the launch. During its flight a rocket can experiment three different motions: rotation, coning and nutation.

The rotation of the rocket around its z-axis, i.e. longitudinal axis, is called roll rotation. It is also often called spin, and is induced on the rocket on purpose in order to give the rocket gyroscopic stability. Spin will reduce trajectory potential dispersion even if subjected to lateral acting forces, like thrust or bad position of fins. The typical spinning for a sounding rocket is between 0.5 rps and 15 rps, being 6-7 rps the typical spinning frequency [18]. In order for the rocket to be stable during flight, the elevation of the launcher should be orientated against the wind. The wind will hit the nosecone of the rocket, leaving it in the disturbed position of Figure 1.3. If we add to this the spin of the rocket then it will arrive to an equilibrated position, followed

by an oscillation, like the one of the third image of Figure 1.3, which makes the rocket to be stable [19]. This is called coning, and although it can bring stability, it can also be dangerous. If the coning is big, the rocket won't follow the expected trajectory. The third motion is called nutation. It is a fast and small coning around the longitudinal axis of the rocket, typically of the same frequency as the spin, which effect can be seen as small circles drawn by the nosecone tip in the sky.

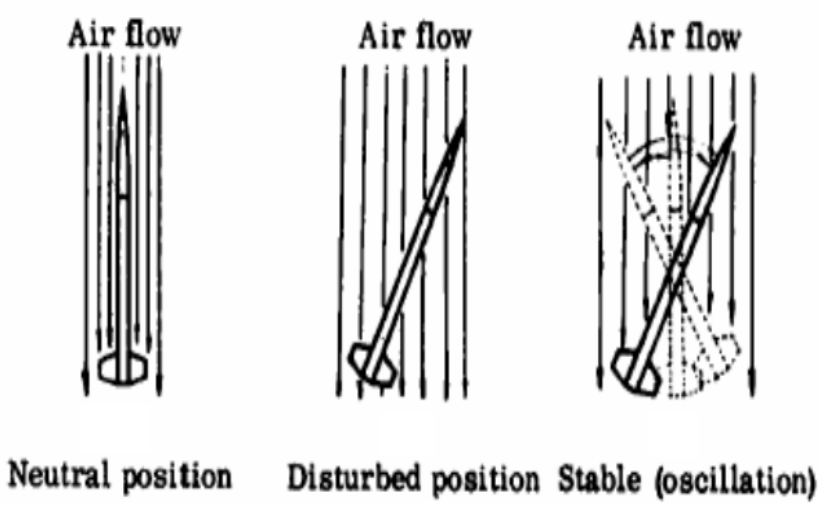

Figure 1.3: Rocket stability. Credit: [19]

1.3 Earth's magnetic field

The Earth acts like a big spherical magnet, since it is surrounded by a magnetic field. This field can be approximated at the Earth's surface by a magnetic dipole placed at the Earth's center, but tilted about 11° with respect to the Earth's rotation axis. The line that crosses the Earth's center along the dipole axis intersects the surface at two points, known as the geomagnetic poles. These poles are not the same as the magnetic poles because the line that joins the magnetic poles does not pass through the Earth's center. The magnetic poles are the places at the surface where the field is vertical. These two poles do not coincide because the magnetic field is not perfectly described by the dipole approximation [4].

At any point the Earth's magnetic field can be described by various elements, which are shown in Figure 1.4. The intensity of the total field is

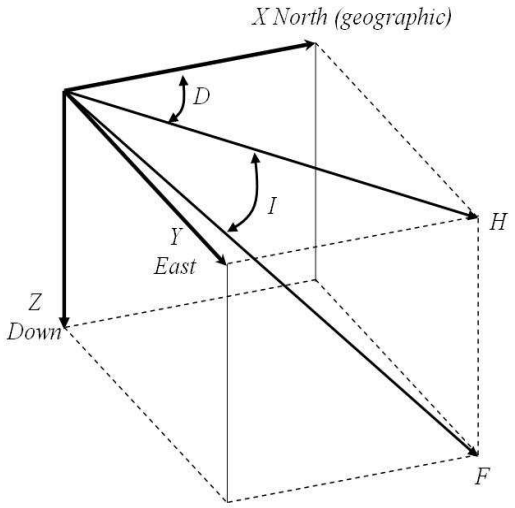

Figure 1.4: Main elements of the geomagnetic field. Credit: [4]

represented by F, and is described by its horizontal component H and its vertical component V. The horizontal component H is described by its north component X and its east component Y. Magnetic declination D is the angle between magnetic north and true north, and is measured positive eastwards. Magnetic inclination I is the angle between the total field and the horizontal plane, and is measured positive into Earth.

Different magnetic fields interact with each other, and are superimposed forming the geomagnetic field. The portion of the geomagnetic field generated internal to the planet in the Earth's outer core is 90% of the total field, and it is referred as the Main Field. It varies slowly with time and there are some mathematical methods to model it, such as the World Magnetic Model (WMM). WMM is a product of the United States National Geospatial-Intelligence Agency (NGA), and represents only the field generated in the Earth's fluid outer core. The 10% left of the geomagnetic field is generated by external currents in the ionized upper atmosphere and magnetosphere, which vary rapidly with time [20]. Therefore the geomagnetic model WMM would give us a value of the magnetic field in one point, which will not be exactly the real value of the field at that point, but very approximated. The way of presenting the elements of the geomagnetic field is in isomagnetic charts, maps with contours of equal values of a magnetic element. We can find 3 different maps: the isogonic map for presenting the declination, the isoclinic for the inclination and the isodynamic for equal intensity [4]. The main field intensity obtained by the WMM is shown in Figure 1.5

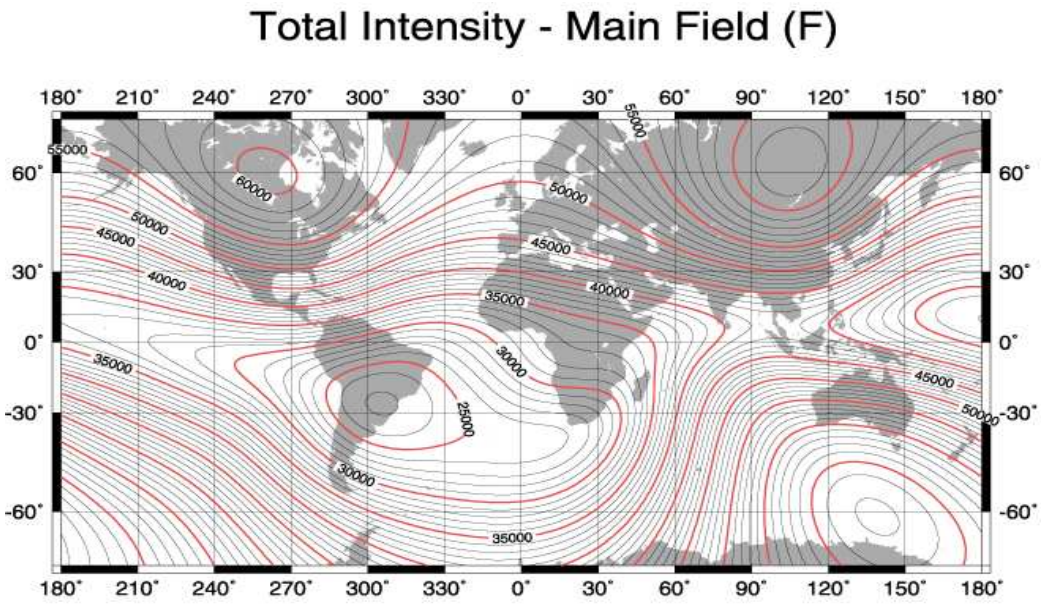

Figure 1.5: Isodynamic chart presenting the total intensity of the Earth's main field. Contours are labeled in nT, and contour interval is 1000 nT. Credit: [20]

Chapter 2

Mini-Dusty project

The Mini-Dusty (MD) rocket payload is a multi-instrumented miniaturized rocket payload, created to investigate the conditions in the atmosphere between 50 to 100 km, with special emphasis on the mesopause region ∼85 km. This research was mainly centered in the relation between NLC particles and PMSE, explained in section 1.1.2. The first experiment, which took place in 1994, revealed that NLC and PMSE were associated with large quantities of charged dust [7]. The next launches in 1999 had the goal of investigating these dust charges, positives and negatives, during the different stages of NLC and PMSE. Scientists were searching also for a relation between the dust layers and the strength of PMSE [21].

Unfortunately, the booster used at the beginning is no longer produced, and other motors are being tested for future use. Due to the bad behavior of the new motors, the last rocket launched, Mini-Dusty 13, was carrying more accelerometers, and also magnetometers in order to provide more information about the dynamical behavior of the rocket during flight.

2.1 Original Mini-Dusty rocket

A rocket is composed of the payload and the booster. The booster used in the original project was the Viper IIIA booster. The payload, i.e. front part of a rocket which carries instrumentation, for achieving these scientific goals is called Mini-Dusty payload. It comprises the power supply, the power control, the pyrotechnics, the transmitter, the pulse code modulation (PCM) encoder, magnetometers, and the scientific equipment, which is composed of electrometers, and 6 probes [22]. The payload has a diameter of 54 mm, a length of 1465 mm, and a weight of 9.3 kg [21].

2.1.1 Housekeeping equipment

The housekeeping equipment comprises the instrumentation to monitor the status ("health") of the rocket, such as the power supply, the power control, the pyrotechnics, the transmitter, the magnetometers, and the temperature sensors, which are used to monitor the temperature on the payload's board and also outside. It also collects data (mostly digital but also analogical) from instruments, encodes it with a PCM encoder and transmits it to ground by telemetry.

The power supply is usually a Li-ion battery with a 7.2 V output and a maximum current of 1.5 A [22]. The charging circuit has a constant current of 1.1 A. The power supply is brought into operation only some seconds before the launch. Before launch the supplies from ground feed the payload through the umbilical cable, which separates from the rocket when it lifts off.

The power control board is in charge of charging the power supply for the circuits, and also of the safety fuse for pyrotechnics, which will be blown $\sim$30 s before the launch. The charge of the power supply is made by means of the umbilical cable [22].

The scientific probes have to be in contact with the atmosphere, but they cannot be launched without any protection. That is the reason for a pyrotechnic system to eject the nosecone and leave the probes in contact with the air. Each pyrotechnic system is formed by two small charges, called squibs. There are a total of 8 individual circuits, which will split the nosecone and open the instrument doors. They are controlled by the PCM encoder, which sends the electrical signal that makes the squibs work [22]. The pyrotechnics are synchronized with the lift off, and the sequence will go as follows: the doors will separate 44 s after lift off, and the nosecone will separate 62 s after lift off.

The magnetometers are located in the motherboard. Usually, only two magnetometers are located in the Mini-Dusty payload, and they are used to determine the orientation, and the spin of the rocket [22]. They measure magnetic fields and convert them to a differential output voltage, which indicates both field magnitude and direction. Knowing the magnetic field being measured by the rocket, its orientation can be obtained, since the Earth's magnetic field is well known.

We can see the drawing of the housekeeping instruments' location for a Mini-Dusty payload in Figure 2.1 (a), and also the real motherboard of the Mini-Dusty 08 and 09 rocket in Figure 2.1 (b).

The information of the magnetometers, and electrometers is coded by a PCM encoder and transmitted to the antennas on a frequency of 2.2795 GHz (S-Band) [22]. The antennas are located on the dart fins, therefore the coded

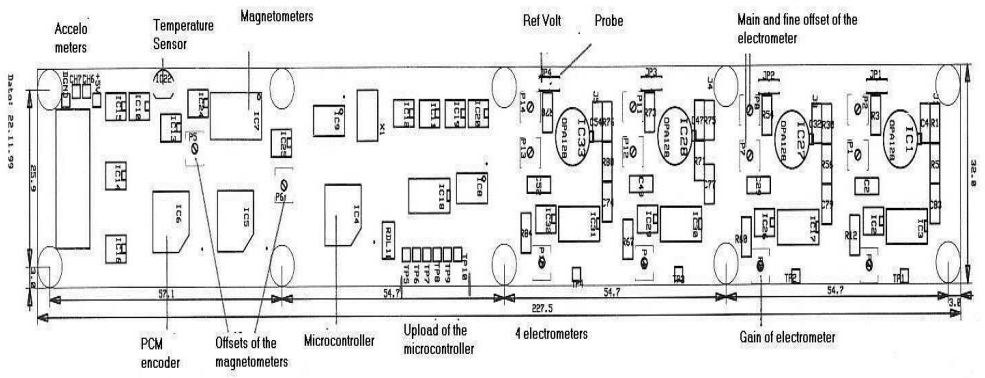

(a) Scheme. Credit:[22]

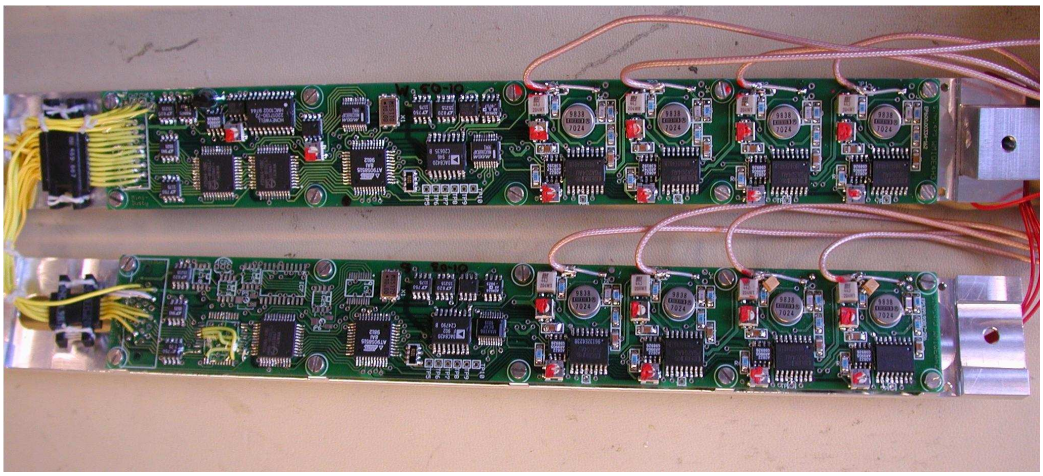

(b) Real motherboard of MD-08. Credit:[23]

Figure 2.1: Motherboard of a Mini-Dusty payload.

signal should be split in 4 different signals that feed each antenna. This is done by the feeding divider shown in Figure 2.2. There is a 90-degree phase shift of the signal, between each fin.

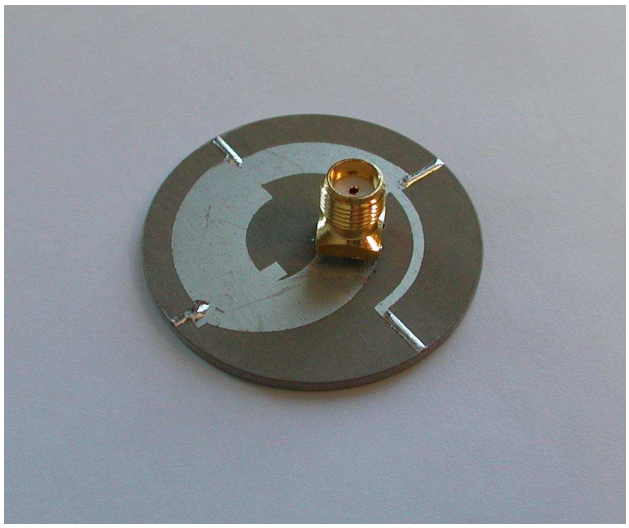

Figure 2.2: Feeding divider. Credit: [23]

2.1.2 Scientific equipment

The scientific equipment for the Mini-Dusty rocket comprises 6 probes, and a total of 8 electrometers. The probes are: the dust probe, the ion and electron probes, the ozone photometer, the temperature probe, and the Faraday probe.

The dust probe's main goal is to measure currents from impacting dust particles. For achieving this it was design a 2-grid system and an impact plate, which we can see in Figure 2.3. The first grid is set at +6.2 V in order to deflect ambient ions and absorb electrons, so only dust particles (high energies) and no mesospheric plasma will penetrate the first grid. The second grid is set at -6.2 V and the dust collector (impact plate) is set at -2.0 V. The current measured in the second grid and the impact plate is caused by direct impacts, and if the impacts are energetic enough, also secondary impacts will contribute too [7], [22].

The ion probe is a grid on an arm set to -6 V for measuring ions and the electron probe is equal to this one but set to +6 V for measuring electrons. They are $\sim$7 cm long [22], and they are used for investigating the relationship between the dust density, and charge, with the electron and ion density. This

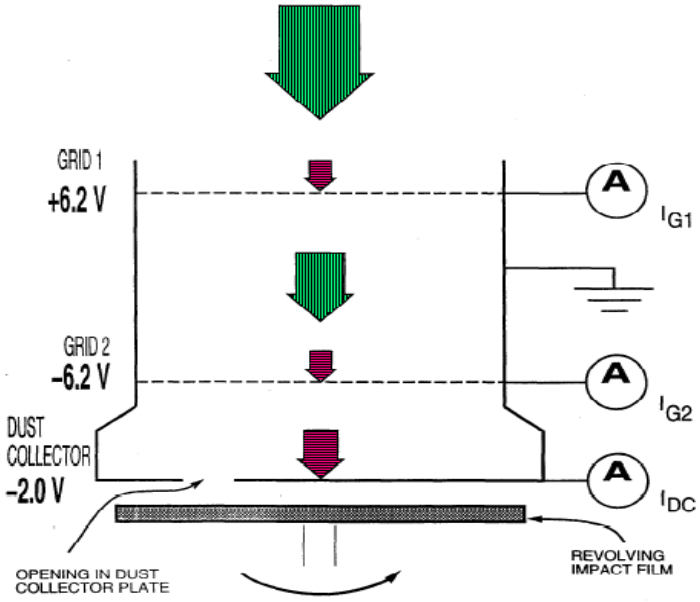

Figure 2.3: Scheme of the dust probe. Credit: [7]

will also give some information about how this densities are related with the PMSE strength [21]. An image of the dust probe with the ion and electron probes is shown in Figure 2.4.

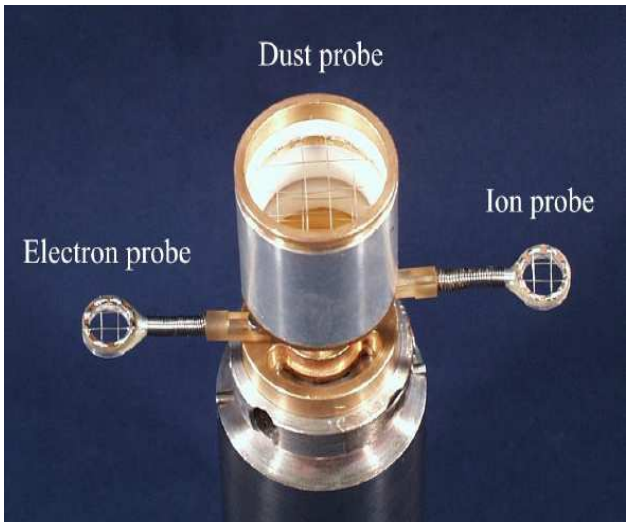

Figure 2.4: Dust, ion and electron probes. Credit: [22]

Sometimes another electron probe, such as the halo probe can be used. The halo probe is a ring set to +6 V, and extended out in front of the dust probe after the nosecone is released, as we can see in Figure 2.5. This probe minimize the rotational effect that suffers the other type, and allows dust to enter to the bucket.

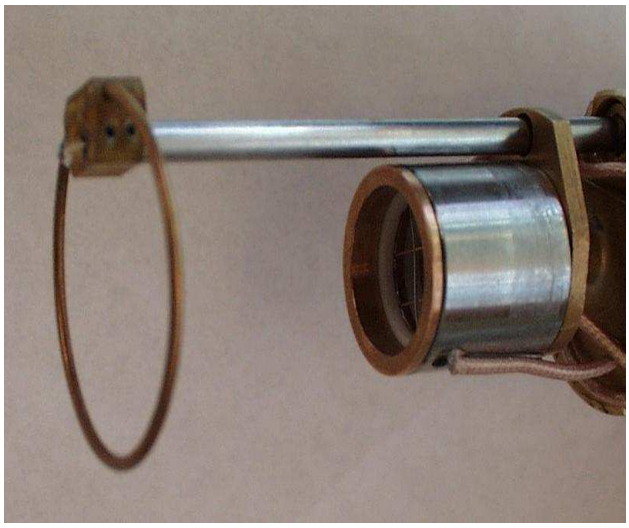

Figure 2.5: Halo electron probe and dust probe. Credit: [23]

The ozone photometer measures the light in three different wavelengths: 250 nm, 280 nm and 300 nm, the three in the ultraviolet region of the spectrum. The ozone density can be determined by the amount of light captured by the three different channels because the ozone affects in different way to these wavelengths [22]. An image of the ozone photometer is shown in Figure 2.6.

The temperature probe has 2 lobes: one with a positive voltage and the other one with negative voltage, as we can see in Figure 2.7. The electron density can be calculated from the measured electron temperature [22].

The Faraday probe bases its operation in the Faraday Effect, also called Faraday rotation. A plane-polarized wave can be decomposed into two circularly polarized waves. Given these two rays of circularly polarized light, one with left-hand and the other with right-hand polarization, the one with the polarization in the same direction as the electricity of the magnetizing current travels with greater velocity. This means that the plane of linearly polarized light is rotated when a magnetic field is applied parallel to the propagation direction [24]. This effect is caused by free electrons and can be characterized as a difference in the refractive index seen by the two circu-

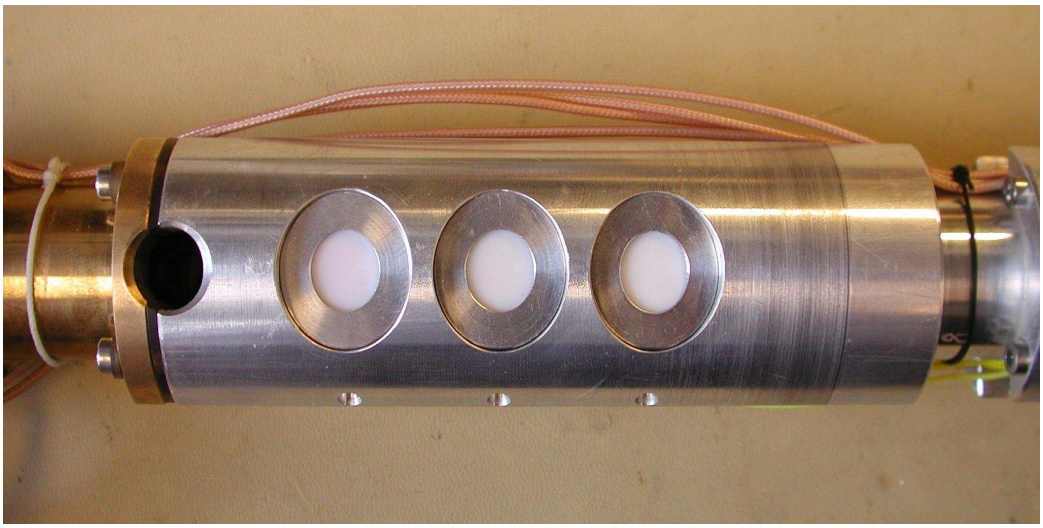

Figure 2.6: Ozone photometer in MD-08 and MD-09. Credit: [23]

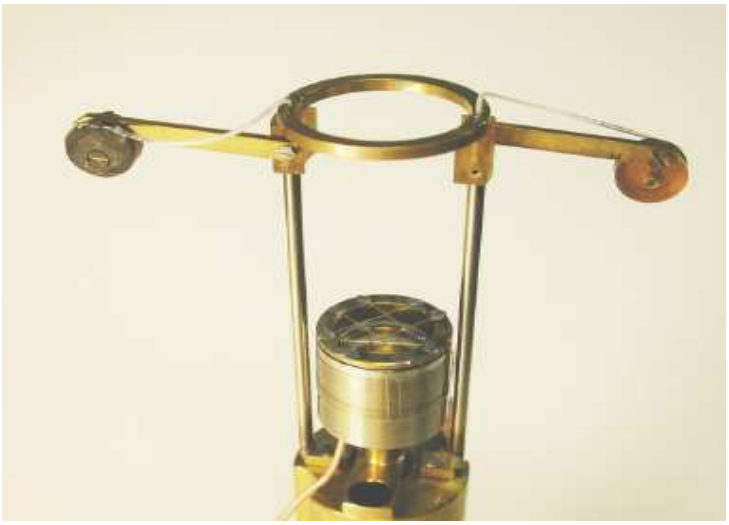

Figure 2.7: Temperature and dust probes. Credit: [22]

larly polarized propagation modes. According to this, if a wave is sent from a ground station and the probe takes measures of this rotation as it travels through the beam, the amount of rotation is a measurement of the electron density of the plasma [22]. We can see the probe in Figure 2.8.

Each electrometer measures the electric current produced by each probe, therefore we should have at least 6 electrometers. There are a total of 8 elec-

Figure 2.8: Faraday probe. Credit: [22]

trometers, 4 located on the motherboard, and 4 located on the slave board. All of them have a sensitivity of 10^{-13} A, but the electrometer located furthest from the digital circuits will receive less effect from them, and therefore it will be the most sensitive in practice [22].

2.1.3 Assembly of the payload

Here in Figure 2.9 we can see the different parts to mount once the probes and instrumentations have been put together. The instruments can be seen at the bottom of the image in orange and grey. The heat insulation is drawn in light yellow, and the outer hull is above the heat insulation and drawn in dark grey. The tail section is in the left upper corner of the figure, and the nosecone is shown in light green. The doors are painted in dark brown.

Before the final assembly, all components and connections should be checked again, and looked for damaged wires. During the assembly all the solder-points should be localized and glued tight, all the screws of the inner payload should be tightened by a pressure screwdriver, and the wire should be joined together with tape. Once all these is checked, the first thing to do is to mount the squibs very carefully. Then before putting the heat insulation tube around the probes and electronics, it must be covered with aluminium foil. Once is put around the instruments, it should be aligned and secured with a screw. Some teflon tapes have to be put on the places where the payload has contact with the outer hull. When mounting the outer hull we have

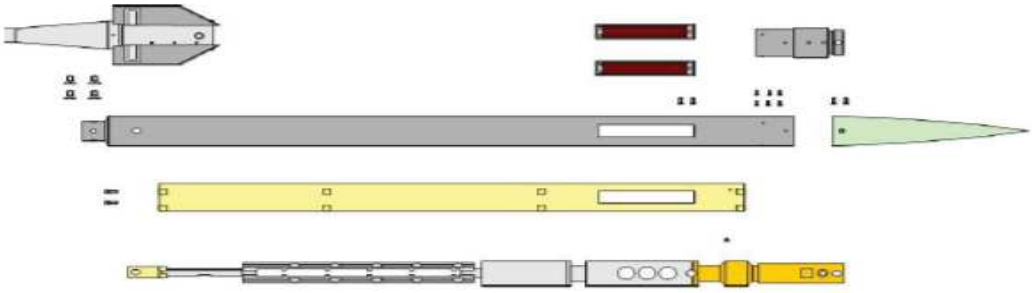

Figure 2.9: Overview of the payload's parts. Credit: [22]

to be carefully with the antenna cable and with the hole for the umbilical cable, and once both things are ok, then we can screw the hull to the rest of the payload. After this we will mount the tail section, but just before the antenna cable should be connected. The tail section should be adjusted with 4 special screws. The last thing to do is to attach the nosecone and the doors, and it should be done carefully because the squibs should be in the correct place in order to work and eject them.

We can see a real payload with the heat insulation already around it, and with the outer hull just besides in Figure 2.10. This process of assembling is the same for every Mini-Dusty payload.

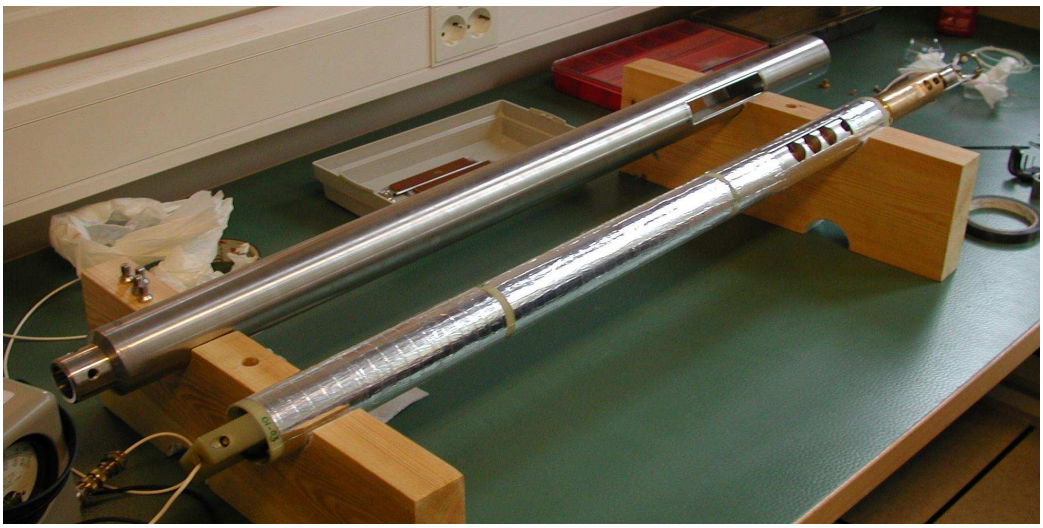

Figure 2.10: Outer hull and payload with heat insulation. Credit: [22]

2.1.4 Booster

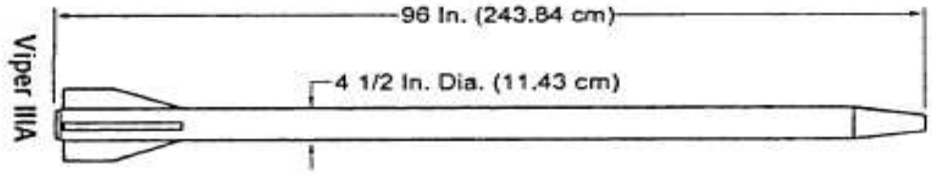

Figure 2.11: Orbital's solid propulsion Viper IIIA motor. Credit: [16]

The original booster selected for the Mini-Dusty payload was a Viper IIIA of size 11.43 cm diameter and 243.84 cm in length, as we can see in Figure 2.11. It contains 25.91 kg of HTPB/AP case bonded solid propellant with a total impulse of 58720 Ns and an average thrust of 24669 N [16].

This booster uses a helical launch rail assembly like the one shown in Figure 2.12 (b). The dart fin tips are guided by the rail on the helix. The helical launcher imparts 6 rps roll rate into the vehicle for minimizing dispersions, which normally happen in unguided sounding rockets [16].

Figure 2.12: Helical launcher. Credit: [23]

2.2 Current Mini-Dusty rocket, MD-13

The rockets with the Viper IIIA booster followed the predictable trajectory, and the launch and payload separation worked well. Unfortunately the Viper IIIA booster is no longer available. This led to the search for other boosters suitable for the Mini-Dusty payload. Two motors, the Excalibur 2 and the RH 200 SV were tried, but turned to make the rocket cone with a very high angle, resulting in a lost in altitude, or even in a totally different trajectory that the expected one. The RH 200 SV is theoretically able to take the Mini-Dusty payload up to 110 km, so some modifications were made in the payload and in the motor to see if it was possible to have a successful launch with that motor. That is why the payload of the last Mini-Dusty rocket launched did not have scientific equipment, but more housekeeping than others.

2.2.1 Housekeeping equipment

The housekeeping equipment is similar to the original Mini-Dusty rocket one, but with some additions. It comprises the power supply, the power control, the pyrotechnics, the transmitter, the PCM encoder, 1-axis and 2-axis magnetometer, and 3 dual axis accelerometers.

The description of the power supply, power control, pyrotechnics, transmitter and encoder is the same as for the original design.

The magnetometers are Honeywell 1- and 2-axis magnetic sensors. The 1-axis magnetic sensor is the HMC1001, which measures the magnetic field in the y axis. The 2-axis magnetic sensor is the HMC1002, which measures the magnetic field in the x and z axis. The x, y and z axis are defined as the normal cartesian coordinates, being z the rocket's longitudinal axis. Both magnetometers have a misalignment of 1.8 mm in the -y direction, because the circuit board is not exactly in the center of the payload. We can see the location of the magnetometers in the board in Figure 2.13 (a), and how they are misalignment from the center once the payload is built in Figure 2.13 (b).

The magnetometers are magnetoresistive sensors which convert magnetic fields to a differential output voltage. They can measure a field range of ± 2 gauss, where $1\ gauss = 10^{-4}\ T$. Their resolution is 27 μgauss [25].

One of the most important processes during the built of the payload is the calibration of the instruments. The magnetometer reads the magnetic field during the rocket's flight, and sends the readings to the ground. These results will be expressed in uncalibrated units, direct values from the A/D converter, and we need to know the relation between them and gauss or nT. The calibration is the process made for obtaining this relationship. The payload is situated inside a room made of coils, without any metallic objects

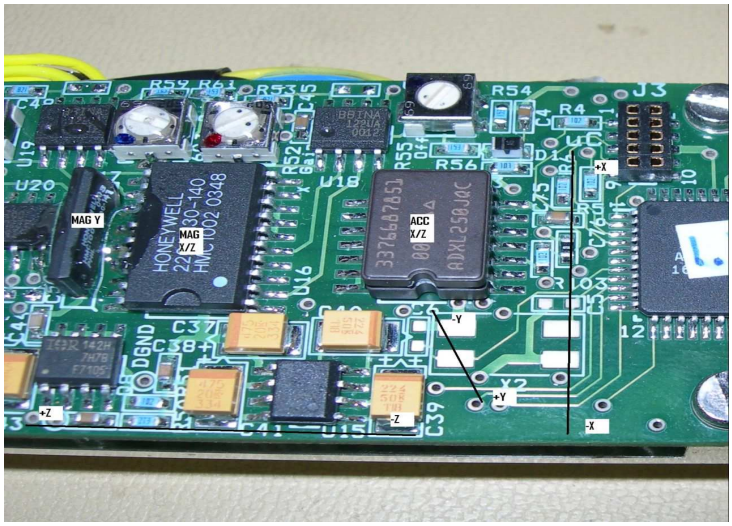

(a) Location.

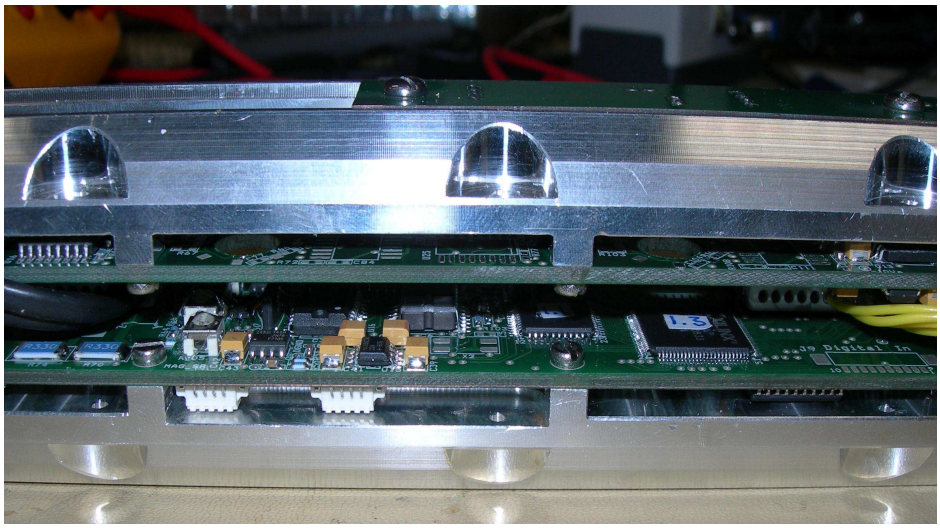

(b) Misalignment.

Figure 2.13: Location of the magnetometers and accelerometer 1 in the MD-13's motherboard. Credit:[23]

which can affect the process. Big coils will be set in 3 different directions in order to build a cubic space, where the payload should be located inside. Then a magnetic field is applied in the z direction and the value read from the A/D converter is noted down. There are also some things to adjust, e.g. if the y-axis magnetometer shows any value when only a field in the z direction is applied, then we have to rotate the offset potentiometer of the y-axis magnetometer until the reading is the correspondent for a 0 gauss field, and the same applies for the x-axis magnetometer. This action should be done with a non-metallic screwdriver, in order not to interfere the readings. Then the payload will be located in the y direction and the process will be repeated again, the same will be done in the x direction.

The results from the calibration of the MD-13 rocket are illustrated in Table 2.1.

Magnetic Field (nT)	x A/D	y A/D	z A/D
50840	3740	3683	3646
0	2080	1994	2015
-50840	490	396	476

Table 2.1: Relationship between the output of the A/D converter and applied magnetic field in nT. Credit:[23]

The calibration was done without the outer hull, so probably there are some small errors to consider. In Figure 2.14 there are some pictures from the calibration process.

The accelerometers are 3 dual axis accelerometers, ADXL250, from Analog Devices. This is a third generation ± 50 g surface micromachined accelerometer, which resolution is 10 mg and dynamic range is ± 50 g [26]. The accelerometers were not included in the original payload but, since the latest rockets seemed to have suffered a big coning before separation, now the data provided by the accelerometers during the whole flight will be very important for analyzing the dynamical behavior of the rocket. They will provide information about the motion of the rocket, such as its shaking during the burn phase, its acceleration at separation, and the coning angle of the rocket [27]. There will be 3 accelerometers: one x- and z-axis, and two x- and y-axis.

The accelerometers should be calibrated too. The calibration is based on the fact that if we orientate the accelerometer with its sensitive axis to the earth's gravity, it will experience an acceleration of $+1$ g. The reading will be -1 g if the package is rotated 180^o [26]. The process involves turning the accelerometer in 90^o steps, and note down the values. The values for -1, 0,

(a) Coil room

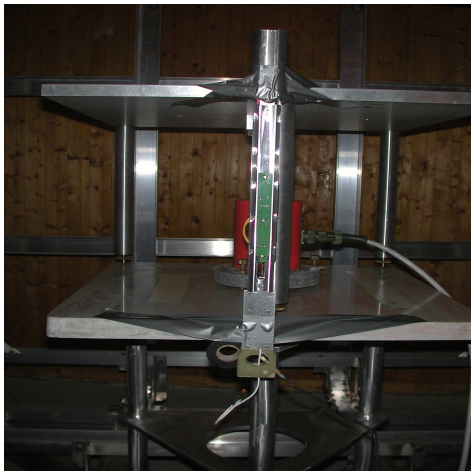

(b) z direction

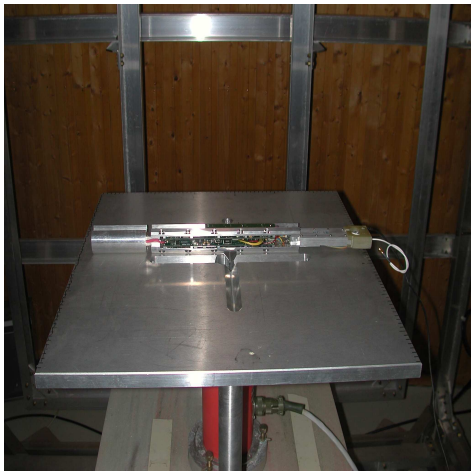

(c) y direction

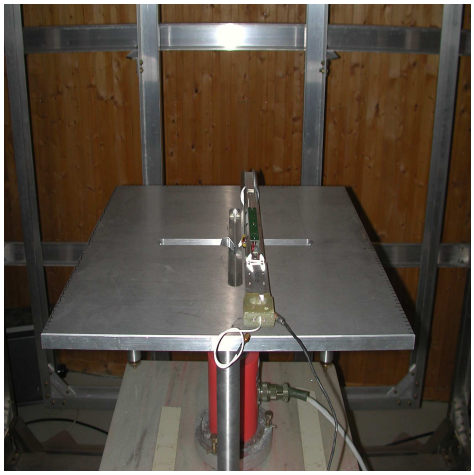

(d) x direction

Figure 2.14: Calibration process. Credit:[23]

and +1 g are then available, referenced to earth's magnetic field. In the case of MD-13 the value adjusted with the potentiometer was the one for 0 g, and the others were noted down. The data was already provided in g.

We can see the x- and z-axis accelerometer, from now on accelerometer 1, in Figure 2.1 (a), one x- and y-axis accelerometer, accelerometer 2, in Figure 2.15, and the other x- and y-axis accelerometer, accelerometer 3, in Figure 2.16.

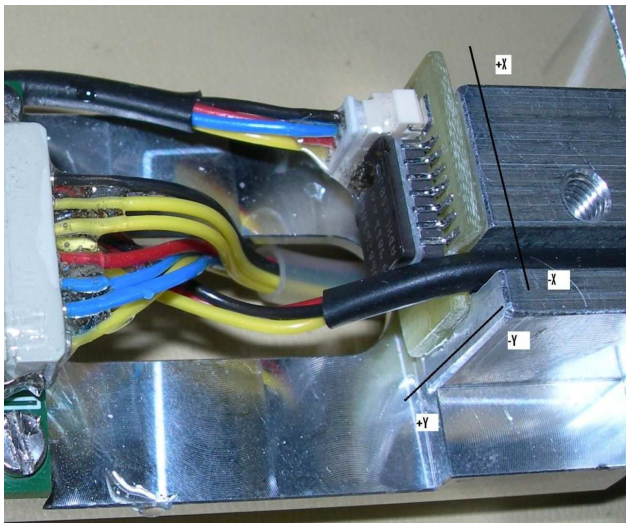

Figure 2.15: Location of the accelerometer 2. Credit: [23]

In Figure 2.15 we can also observe that the accelerometer 2 is misaligned 2 mm in the +x direction, because we see that the cables did not allow a perfect alignment. The accelerometer 1 is also misaligned, but 1.8 mm in the -y direction, because, as explained, the board is not located in the center of the payload.

2.2.2 Scientific equipment

The MD-13 rocket was mainly a technical rocket. The launch of MD-12 went very bad, and the rocket followed a total different trajectory than the predicted one. The scientific instrumentation of the MD-12 was useless, so in order to prevent, just in case the MD-13's launch went bad too, no scientific equipment was put in the payload.

Only two plasma probe arms were mounted under the nosecone, as an additional test of the nosecone separation [27]. We can see them in Figure 2.16.

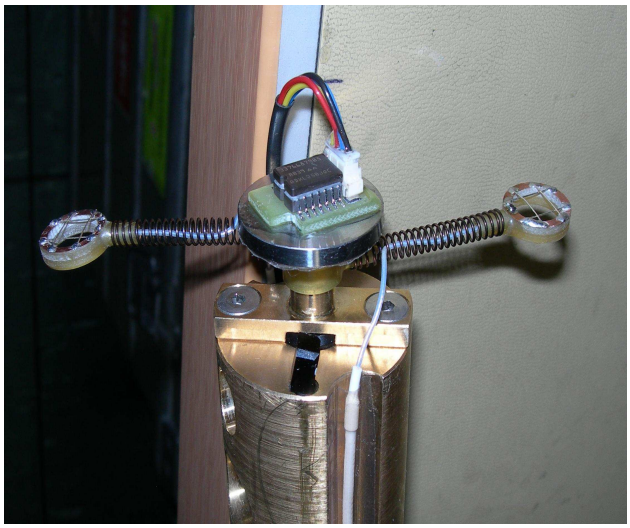

Figure 2.16: Location of the accelerometer 3. Credit: [23]

2.2.3 Booster

MD-13's booster was the Indian RH 200 SV. This is a single stage, unguided, and fin stabilized vehicle. Theoretically it can carry a 54 mm diameter, 1378 mm long and 10 kg payload to an altitude of about 100 km. This motor has a diameter of 207 mm, and uses case bonded HTPB propellant system. The nominal burning time is 10 s. The lungs are retractable, which minimizes drag after the lift off [27].

This booster is much bigger than the Viper IIIA, and heavier. Whereas the Viper IIIA weighted ∼36 kg and had 114 mm diameter [21], the RH 200 SV weights ∼140 kg and has a 207 mm diameter [27]. The propellant's weight of the Viper IIIA was 25.91 kg, whereas for the RH 200 SV it is 92.25 kg.

Figure 2.17 shows both the payload and the booster of Mini-Dusty 13 in the launcher.

Figure 2.17: Mini-Dusty 13. Credit: [23]

Chapter 3

Presentation of the data from the Mini-Dusty 13 flight

The Mini-Dusty 13 was launched at 23 h 28 min 29 s on March 1st, 2007 in ARR, Norway.

ARR is located at geographic coordinates 69^o 17' N latitude and 16^o 01' E longitude. The range cooperates with European Space Agency (ESA) program and supports orbital satellite operations, sounding rocket and balloon operations.The range covers a large impact area in the Norwegian Sea, and it offers an extensive system of ground observations, working together with ALOMAR, the arctic lidar observatory for middle atmosphere research.

The telemetry station and the tracking system of the range provided us with the rocket's data sent to ground, and with more information about the trajectory.

Some of the following graphs are the result of directly plotting the data provided by the ARR with MATLAB®.

MATLAB® is a high-level technical computing language and an interactive environment for algorithm development, data visualization, data analysis, and numeric computation. It was created by MathWorks, a company founded in 1984 that has become the leading global provider of technical computing and model-based design software. Using MATLAB®, you can solve technical computing problems faster than with traditional programming languages, such as C, C++, and Fortran. You can use MATLAB® in a wide range of applications, including signal and image processing, communications, control design, test and measurement, financial modeling and analysis, and computational biology [28].

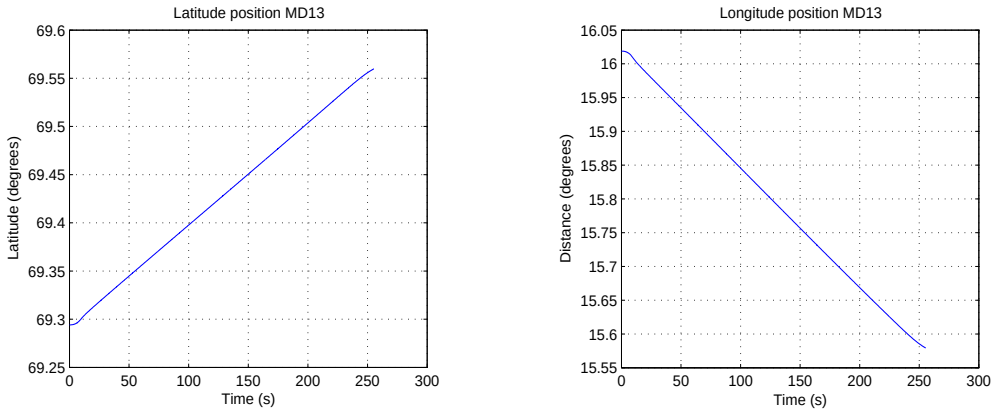

(a) Latitude.

(b) Longitude.

Figure 3.1: Latitude and longitude position of MD-13 during flight.

3.1 Trajectory

The Trajectory and Position System (TPS) from ARR allows to know the latitude and longitude position during the flight. It is shown in Figure 3.1. The MD-13 rocket lifted off at 69º 17 38.76 N 16º 1 7.68 E, and landed at 69º 33 35.28 N 15º 34 45.12 E. The rocket traveled 34.29 km in range, 29.7 km towards north and 17.15 km towards east. This information can be known looking at the graphs of the north and east distance, Figure 3.5, or also calculating how many km/º are the differences in the north and east coordinates. With the latter method, if we assume the Earth's radius as a constant value of 6371 km, we obtain 111.19 km/º, knowing that the Earth's circumference is 360º. This gives 69º 33 40.36 N 15º 51 52.41 E. The result are not exactly the same due to the approximation of the Earth's radius as a constant, because the radius is not constant all over the Earth.

Figure 3.3 shows the ballistic trajectory north-westwards followed by the rocket in its 255.4 s flight. Theoretically the flight had to last 300 s, but it only lasted for 255.4 s. This also means that the apogee was not as high as 103 km, but actually at 75.08 km.

It is known also the elevation, i.e. angle between the velocity vector and the horizontal plane, and the azimuth, i.e. angle between the north and the velocity vector's projection on the horizontal plane measured clockwise. Both are shown in Figure 3.4.

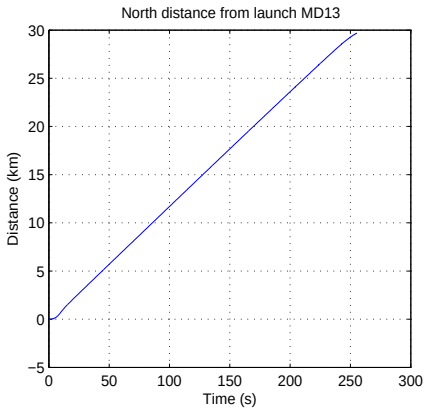

(a) North.

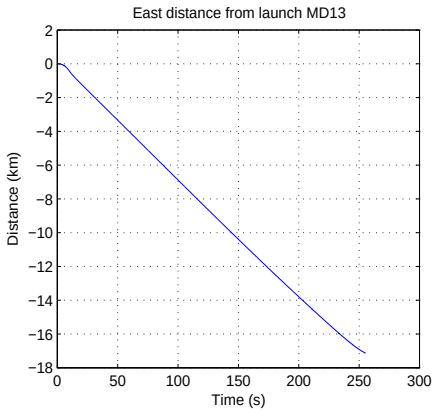

(b) East.

Figure 3.2: North and east distances covered by MD-13.

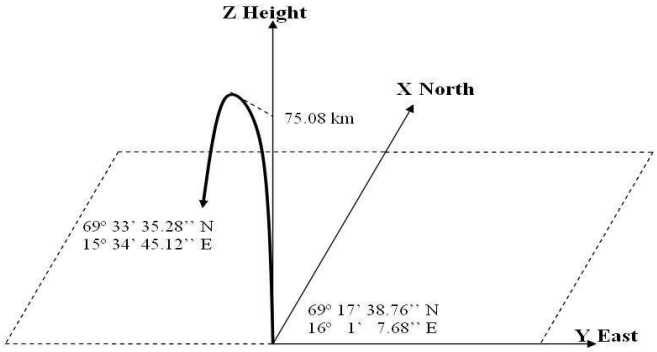

Figure 3.3: Trajectory of MD-13.

3.2 Earth's magnetic field

Information about the Earth's magnetic field in each moment of the rocket's trajectory is also provided. In Figure 3.5 it can be see the north and east components' magnitude of the Earth's magnetic field, and in Figure 3.6 it is observed the vertical and horizontal components, and the total field. The horizontal component is obtained with Equation 3.2.1, and the total component, provided by ARR, can also be obtained with Equation 3.2.2.

$$B_H = \sqrt{B_N^2 + B_E^2} \tag{3.2.1}$$

$$B_F = \sqrt{B_H^2 + B_V^2} \tag{3.2.2}$$

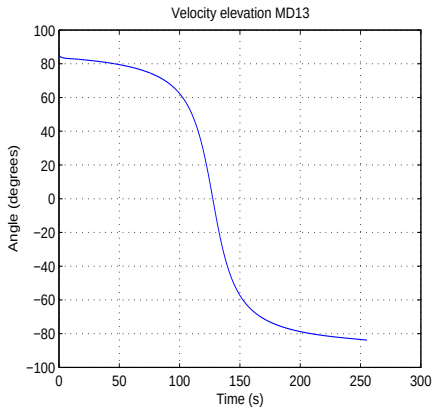

(a) Elevation.

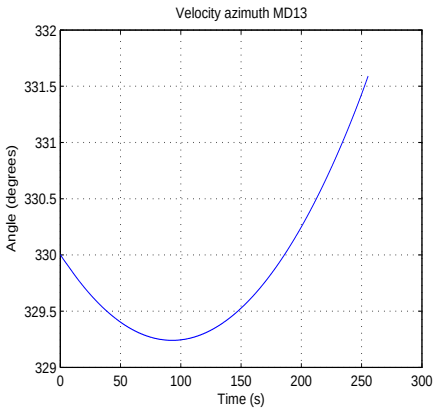

(b) Azimuth.

Figure 3.4: Elevation and azimuth angles of the MD-13.

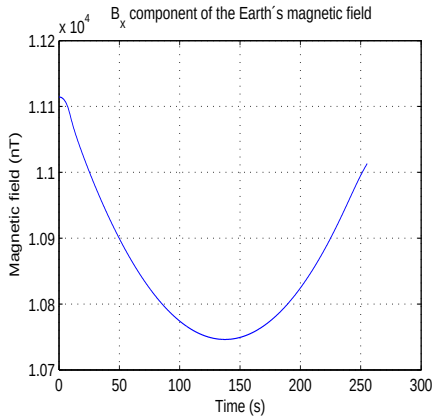

(a) North.

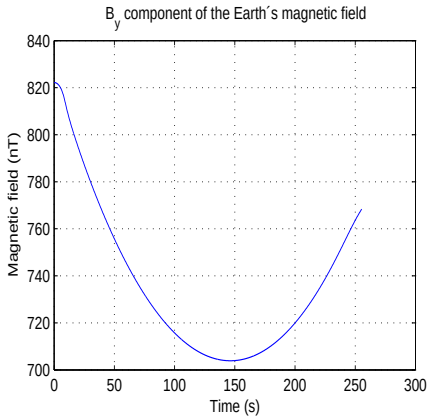

(b) East.

Figure 3.5: North and east components of the Earth's magnetic field in nT for the whole trajectory of MD-13.

The values for the magnetic declination, D, and the magnetic inclination, I, are shown in Figure 3.7. They are obtained with the relation shown in Equations 3.2.3 and 3.2.4

$$D = \arctan B_E/B_N \tag{3.2.3}$$

$$I = \arcsin B_Z/B_F \tag{3.2.4}$$

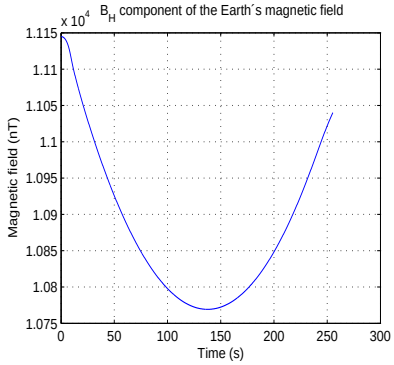

(a) Horizontal.

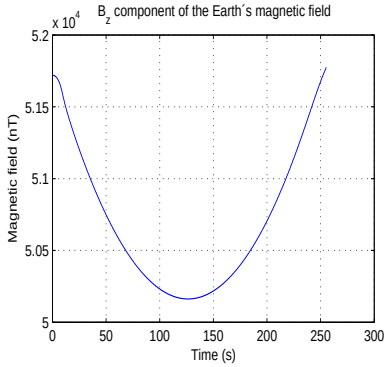

(b) Vertical.

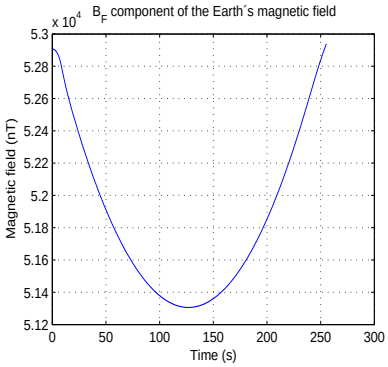

(c) Total.

Figure 3.6: Components of the Earth's magnetic field in nT for the whole trajectory of MD-13.

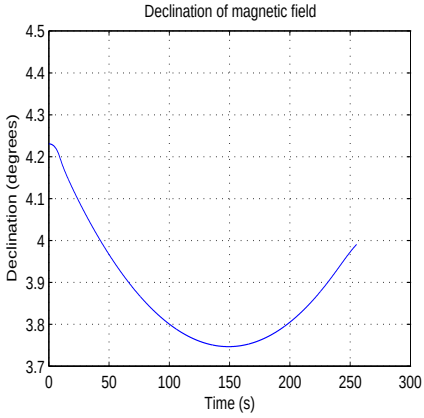

(a) Magnetic declination.

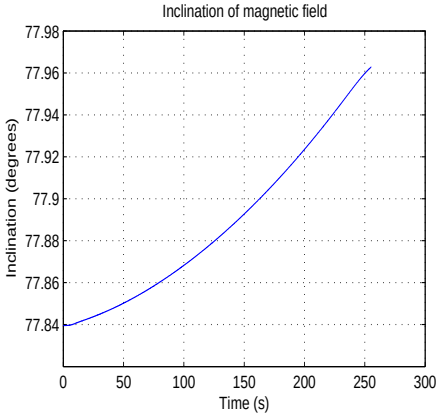

(b) Magnetic inclination.

Figure 3.7: Magnetic declination and inclination for the whole trajectory of MD-13.

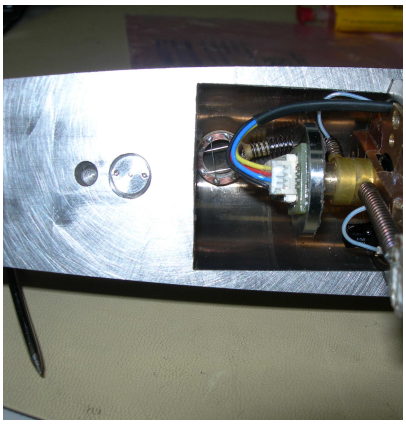

Figure 3.8: View of accelerometer 3 inside the nosecone. Credit:[23]

3.3 Accelerometers

The payload of MD-13 had 3 dual axis accelerometers. Accelerometer 1 measured acceleration in the x- and z-axis, and was located 836 mm away from nosecone tip. Accelerometer 2 measured acceleration in the x- and y-axis, and was located 998 mm away from nosecone tip. Accelerometer 3 measured acceleration also in the x- and y-axis, and was located 215 mm away from nosecone tip. As the nosecone is 301 mm long, accelerometer 3 is located inside the nosecone, as we can see in Figure 3.8.

The files provided consist of the accelerometers' readings from 0 s to 60 s, given in g units. We can see these data in Figure 3.9. All the time data in the graphs are related to the lift off signal, this means that 0 s correspond to the lift off, and this is $\sim$1 s after the ignition.

As we can see from these graphs, from 32 s to 45 s ARR lost track of the rocket. In Figure 3.9 (a) we can see that during the burning phase of the motor the rocket experimented an increasing acceleration being the thrust force higher than the drag force. When the z-axis acceleration is lower than 0 g, this means the drag force is higher than the thrust force, and after 9.3 s (burnout) the drag is the only mechanical force acting on the rocket. Making a zoom in the graph from the accelerometer 1 z-axis, Figure 3.10 (a) we can also see that the payload separation took place at 16.1 s. It was predicted to be 9.3 s, just 1 s before burnout, so it happened later than it was thought. In Figure 3.10 (b) we see the maximum acceleration reached by the rocket, a bit more than 30 g.

Observing Figures 3.9 (e) and (f), it can be seen they are noisier than the ones of accelerometers 1 and 2. One probable reason for this is that the

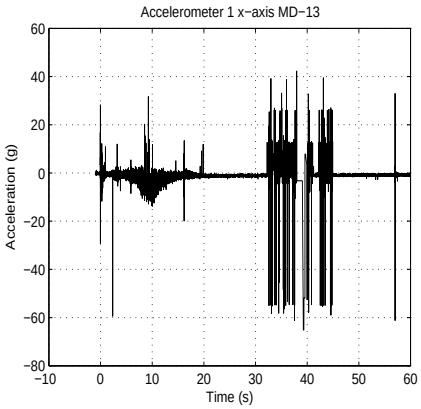

(a) Acc 1 x-axis.

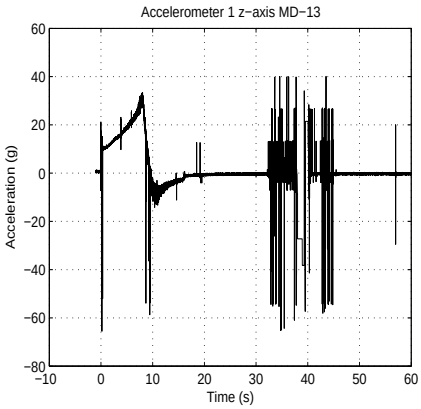

(b) Acc 1 z-axis.

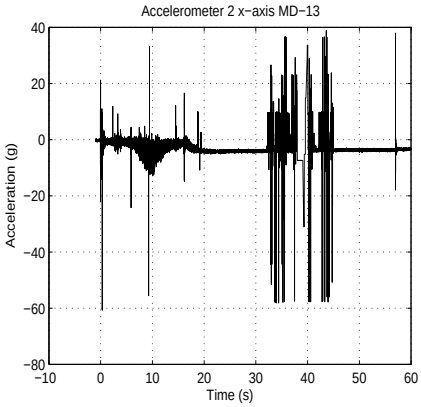

(c) Acc 2 x-axis.

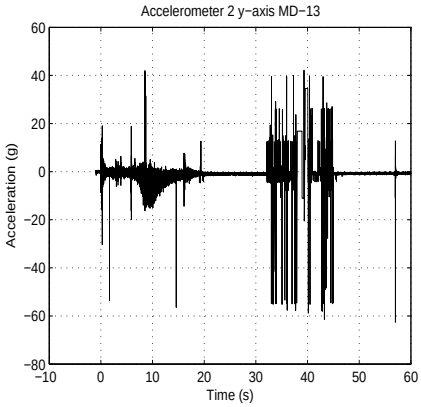

(d) Acc 2 y-axis.

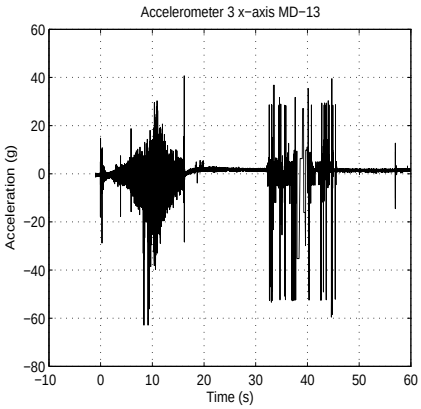

(e) Acc 3 x-axis.

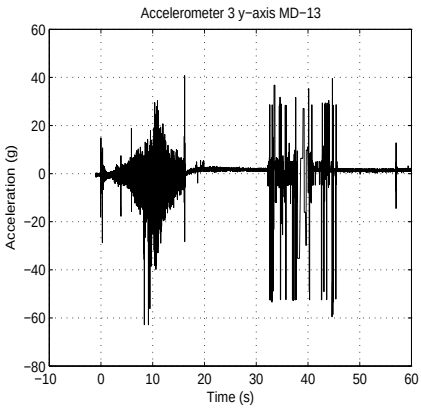

(f) Acc 3 z-axis.

Figure 3.9: Original readings from accelerometer 1, 2, and 3 of the MD-13.

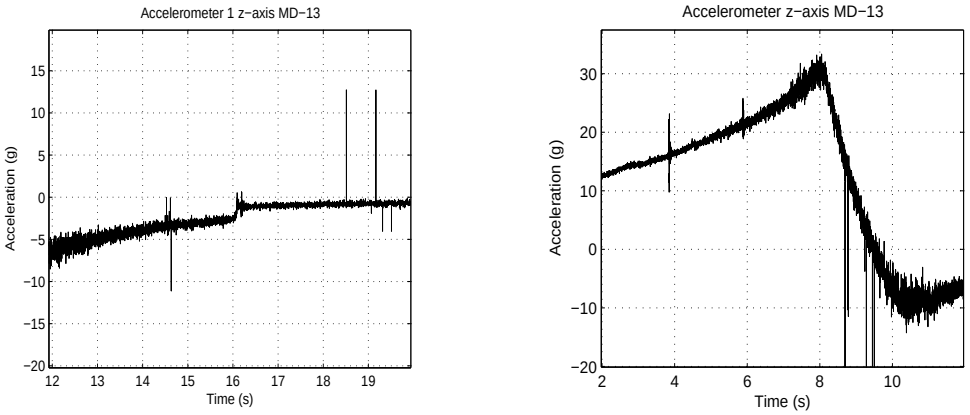

(a) Payload separation.

(b) Maximum acceleration.

Figure 3.10: Zoom in to accelerometer 1 z-axis.

accelerometer 3 was the one located inside the nosecone, and as the nosecone had to be ejected during the flight, it was not as well isolated from the outside as the other accelerometers. Maybe there was some leaking, which could cause some distortion in the readings of accelerometer 3.

3.4 Magnetometers

The payload of the MD-13 had one 1-axis magnetometer and one 2-axis magnetometer. Magnetometer Y was located 818 mm away from the nosecone tip, and measured magnetic field in the y direction. Magnetometer XZ was located 822 mm away from the nosecone tip, and measured magnetic field in the x and z direction.

The files provided consist of the magnetometers' readings from 0 s to 60 s, given in uncalibrated units directly from the A/D converter. We can see these data in Figure 3.11. All the time data in the graphs are related to the lift off signal, this means that 0 s correspond to the lift off, and this is $\sim$1 s after the ignition.

Making a zoom in the graph from the z magnetometer, Figure 3.12, the separation at 16.1 s is clearly seen.

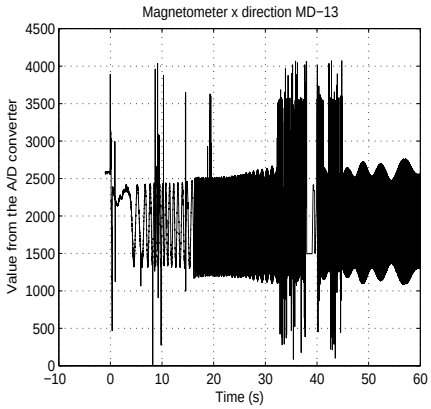

(a) x direction.

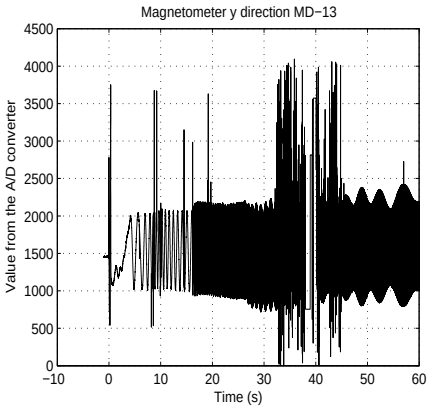

(b) y direction.

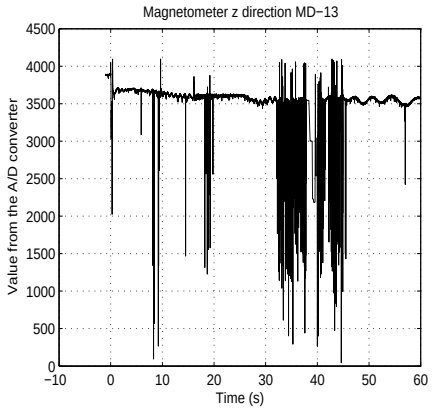

(c) z direction.

Figure 3.11: Original readings from magnetometer x, y, and z of the MD-13.

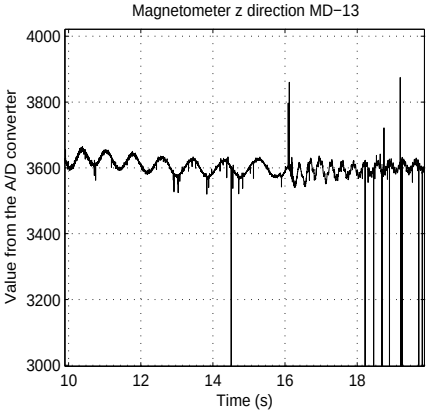

Figure 3.12: Zoom in to the magnetometer z.

Chapter 4

Data analysis and discussions

Due to the problems occurred during the last launches of the Mini-Dusty payloads, the Mini-Dusty 13 had a payload with 3 dual axis accelerometers and 3 magnetometers, when in practice it was designed with 2 magnetometers and no accelerometers. The situation requires such a technical payload, with no scientific instrumentation, in order to comprehend what is happening up there when the rocket is launched.

Until now only qualitative studies have been made. Now there is the necessity of going further in detail, because this last launch was made with a modification of the Mini-Dusty payload and motor. The aims of such a technical launch was to see if the modifications made helped the rocket to have a smoother separation, to see if the rocket behaved better than the last time, if the coning was smaller, or if it reached high enough. Those are the kind of things that should be studied, in general words, the dynamic behavior of the rocket during flight.

This is really important because if this time the motor worked well with those modifications, then probably the next time the payload can carry scientific instrumentation, which is what it was built for. Every kind of information is needed, positive and also negative, in order to see if is it good like this, if some other modifications can be done, or eve if the scientists should start a search for a new motor.

4.1 Preparing data

There are some processes that need to be done to the data in order to obtain good results. If we take a look at Figures 3.9 and 3.11, we can see many values which clearly do not follow the others. These values are called outliers, i.e. data values that do not appear to be consistent with the rest of the data.

This values should be removed.

Also the values from the magnetometers need a change. These values are uncalibrated values directly from the A/D converter, and should be converted to magnetic field units using the data from the calibration table 2.1.

4.1.1 Removing outliers

The program A.1.2 removes the big outliers from the accelerometers' data, and also smooths it using the spline interpolator. The latter can be made for some applications, but the graphs shown in Figure 4.1 have only been processed for removing outliers, and the values for the different parameters of the program are given for each graph. Some small outliers still remain. They can be taken away completely, but for doing that we must afterwards interpolate the result with the spline interpolator because there will be many points without value.

The same process is done for the magnetometers with the program A.1.1. The results are shown in Figure 4.3, where the calibration process has already been done, and the units are in nT.

4.1.2 Calibration of the magnetometers

The process of calibration gave the results shown in Table 2.1. Knowing the relation between uncalibrated values and nT units is linear, the function for making each conversion, shown in Figure 4.2, is calculated as the function that goes through two points. The functions are drawn in Figure 4.2.

Mag	1^{st} point	2^{nd} point	Function
x	(490,-50840)	(3740,50840)	y(nT)=31.2862·x(A/D)-6.617·10^{-4}
y	(396,-50840)	(3686,50840)	y(nT)=30.9340·x(A/D)-6.309·10^{-4}
z	(476,-50840)	(3646,50840)	y(nT)=31.9447·x(A/D)-6.563·10^{-4}

Table 4.1: Functions used to convert from uncalibrated units to nT for magnetometers of MD-13.

In Figure 4.3 is shown the magnetometer data, without outliers and already converted to magnetic field units, nT. The program used for calculating the converted units can be found in A.2.1.

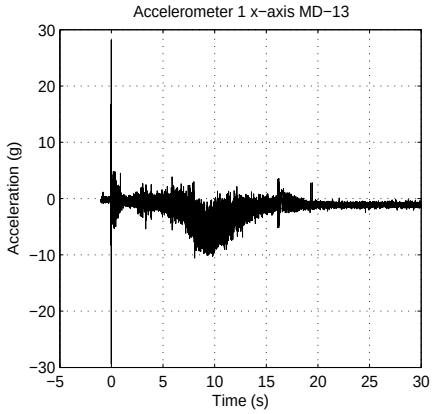

(a) Acc 1 x-axis. mult=1.9, sep=2

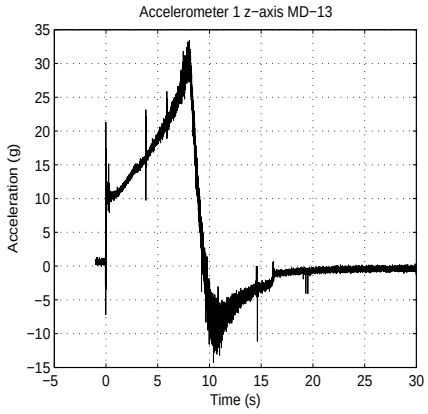

(b) Acc 1 z-axis. mult=1.5, sep=0.5

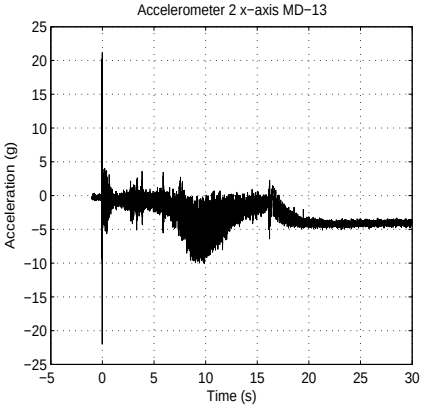

(c) Acc 2 x-axis. mult=1.9, sep=2

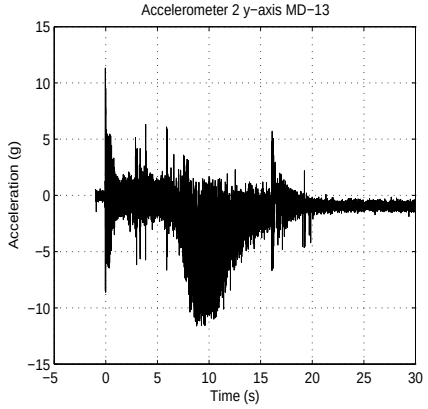

(d) Acc 2 y-axis. mult=2.3, sep=2

Figure 4.1: Readings from accelerometer 1, 2, and 3 of the MD-13 without outliers. t=1

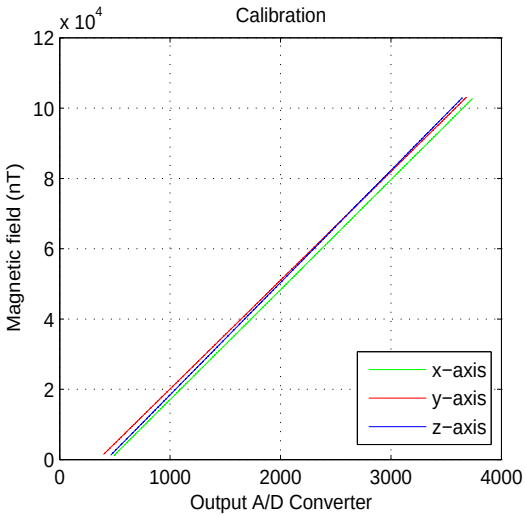

Figure 4.2: Calibration conversion for magnetometers of MD-13.

4.2 Motion during flight

During its flight a rocket can experiment three different motions: rotation, coning and nutation. The rotation of the rocket around its z-axis, i.e. longitudinal axis, is called roll rotation. It is also often called spin, and it is induced on the rocket on purpose in order to give the rocket gyroscopic stability. The wind will hit the nosecone of the rocket, leaving it in the disturbed position of Figure 1.3. If we add to this the spin of the rocket then it will arrive to an equilibrated position, followed by an oscillation, like the one of the third image of Figure 1.3, which makes the rocket to be stable [19] .This is called coning. The third motion is called nutation. It is a fast and small coning around the longitudinal axis of the rocket, typically of the same frequency as the spin, which effect can be seen as small circles drawn by the nosecone tip in the sky.

4.2.1 Frequencies of rotation

Before separation

Before separation the rocket experiments two motions: spinning and coning. We can see these two motions easily by looking to the magnetometer data. The rocket's spin is visible in the data from the x and y magnetometers, because we see a sinusoidal variation. The spin makes the x and y magnetometer sometimes look to a maximum and sometimes look to a minimum.

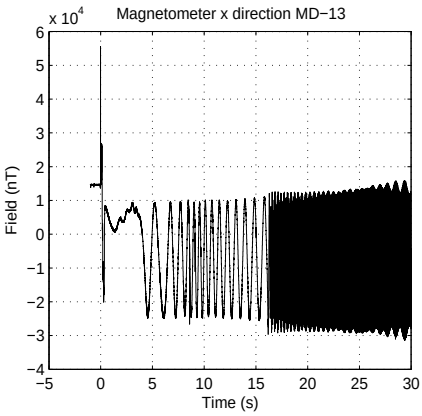

(a) x direction. mult=1.6, t=1

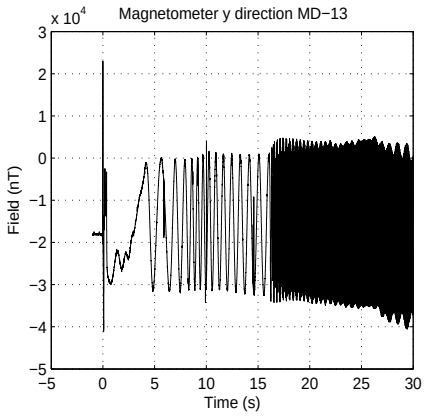

(b) y direction. mult=1.6, t=1

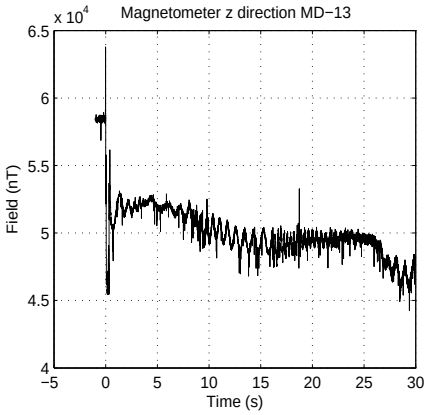

(c) z direction. mult=1, t=1

Figure 4.3: Readings from magnetometer x, y, and z of the MD-13 without outliers and calibrated. sep=2, s=16.1

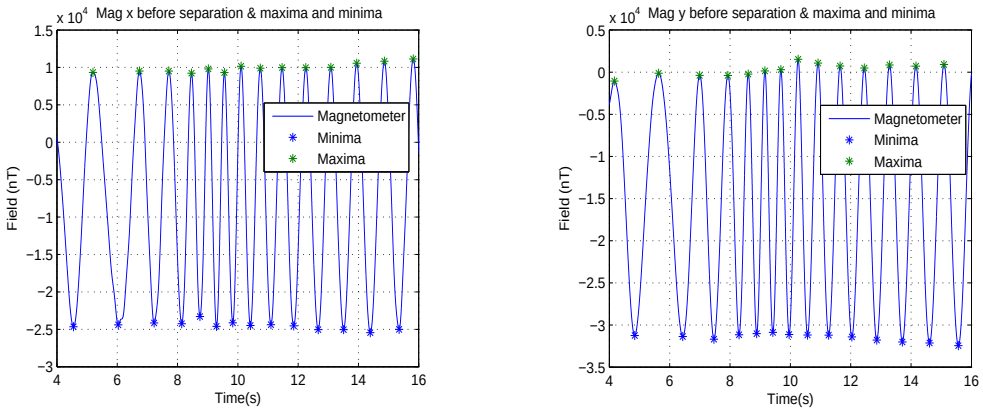

(a) x direction. mult=1.6

(b) y direction. mult=1.8

Figure 4.4: Maxima and minima values in the magnetometer readings from 4 s to 16 s. s=16.1, sep=2, t(1)=240, t(2)=8

The spinning frequency can be obtained from these data. First the program A.1.1 is used to smooth the data, in order to make easier the task of selecting maxima and minima, and afterwards maxima and minima are obtained using the program A.3.1. The result of these two processes is shown in Figure 4.4. Once the singularities are obtained, the calculation of the frequencies is done by A.3.2, and the single frequencies can be interpolated in order to obtain the spinning frequency shown in Figure 4.5.

The rocket's coning is visible in the z magnetometer. The rocket's spinning does not affect the readings of the z magnetometer, so the variation on the z magnetometer is due to the coning motion. The process for obtaining the coning frequency is the same that for the spinning frequency, but using the z magnetometer instead. The results are shown in Figures 4.6 and 4.7.

In Figure 4.7 is illustrated the phenomena of lock of frequencies. Before separation, the spinning and the coning frequencies are very similar. This phenomena makes the x- and y-axis accelerometers measure an increasing magnitude (negative sign) while the thrust is bigger than the drag, and a decreasing magnitude while the drag is bigger than the thrust.

After separation

After separation the rocket experiments 3 motions: spinning, coning, and nutation. The process for calculating the spinning frequency is the same than before separation. The results are shown in Figure 4.8, where (a) is the result directly from joining the frequencies obtained with the maxima and minima, and (b) is the smoothed graph.

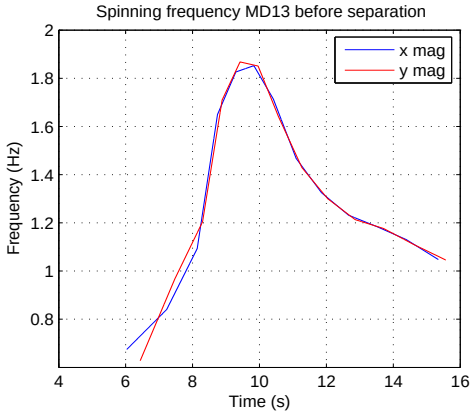

Figure 4.5: Spinning frequency before separation obtained with x and y magnetometers.

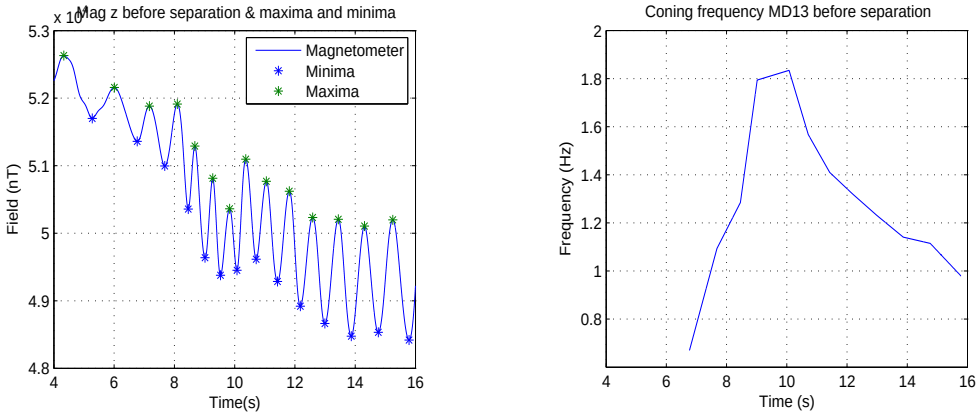

(a) z direction. mult=1

(b) Coning frequency

Figure 4.6: Maxima and minima values in the magnetometer z readings from 4 s to 16 s when s=16.1, sep=2, t(1)=490, t(2)=8, and coning frequency before separation

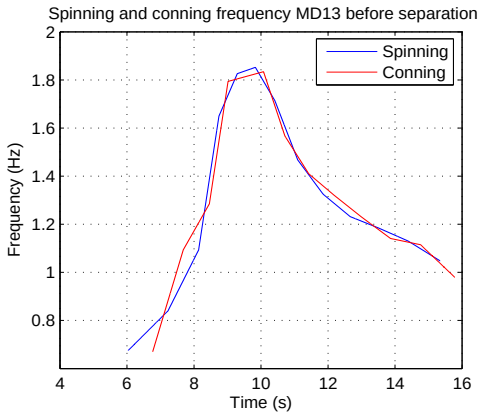

Figure 4.7: Spinning and coning frequencies before separation.

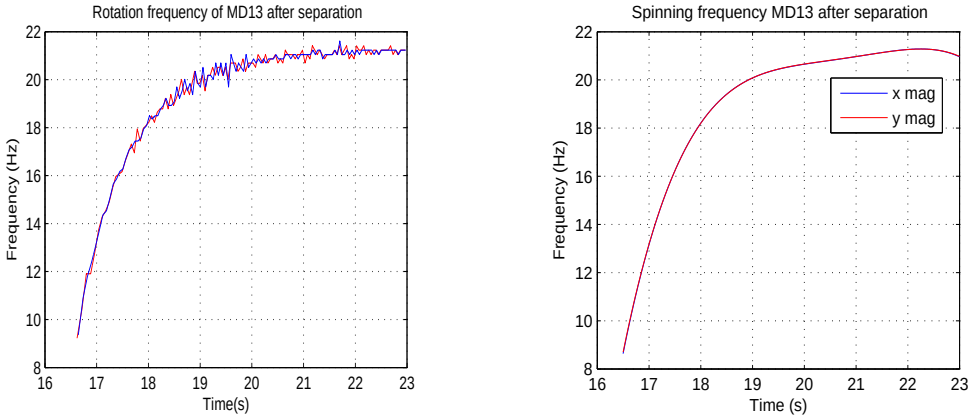

(a) Original

(b) Smoothed

Figure 4.8: Spinning and coning frequency of the MD-13 after separation

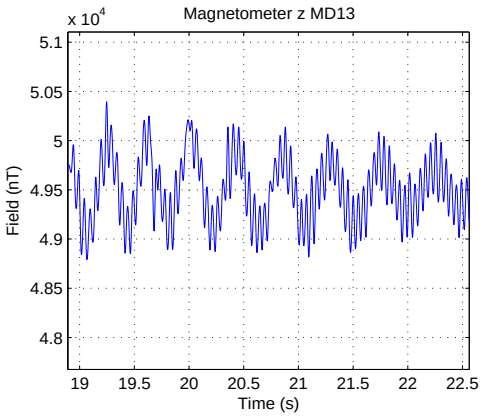

Figure 4.9: Nutation in MD-13 after separation.

The rocket's nutation is visible in the z magnetometer. If there was no nutation the z magnetometer would only have the slow variation related to the coning, however, it also has a faster variation. This quick variation is due to the nutation, and it is shown in Figure 4.9. The nutation's frequency can be seen in Figure 4.10 (b).

The coning frequency can be obtained also as before with the exception of the period between 22 s and 28 s which was interpolated due to complications for finding the maxima and minima. The frequency can be seen in Figure 4.10 (a).

Plotting together the nutation and the spinning frequency, Figure 4.11, it is clear that they are very similar. This is something common to find in such sounding rocket's flights. All the three motions act in a way that the nosecone tip draws small waves around a circle centered in the velocity axis, which is due to the coning motion. The rocket rotates around the main velocity axis much slower $\sim$3 rps than around its longitudinal axis, $\sim$20 rps, which produces the small waves around the circle.

4.2.2 Calculation of the center of gravity

One of the effects of the nutation motion is that the 3 accelerometers see very different accelerations after separation. In Figure 4.12 (a) are shown the three x-axis accelerometers after separation, and in (b) the two y-axis ones. Without the nutation, the data would only vary up and down around 0 g, however, the nutation acts as a small coning but faster. As the frequency is high, is easy to get a few g of difference between them.

Mean values for these x-axis accelerometers after separation are -1.1205 g

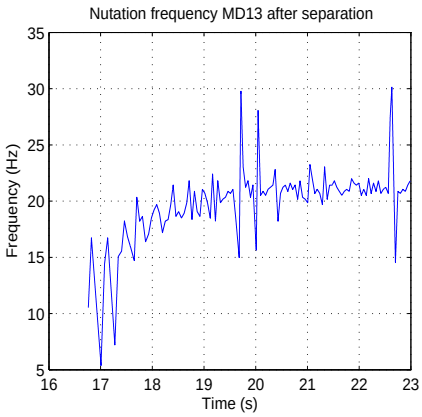

(a) Nutation

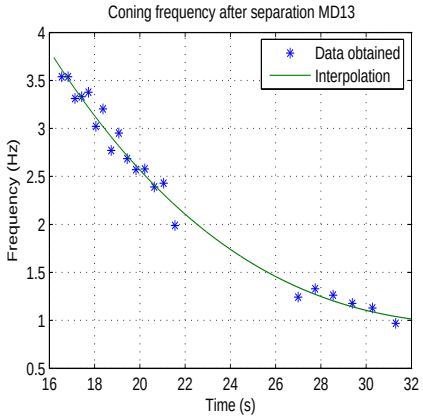

(b) Coning

Figure 4.10: Nutation and coning frequency of the MD-13 after separation

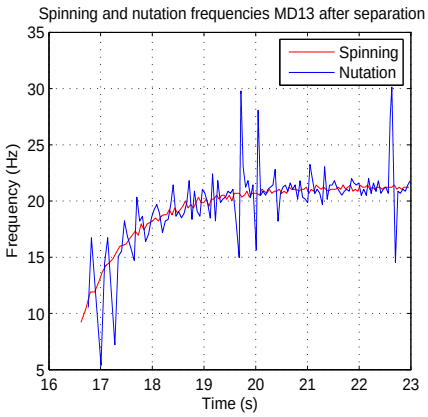

(a) Original

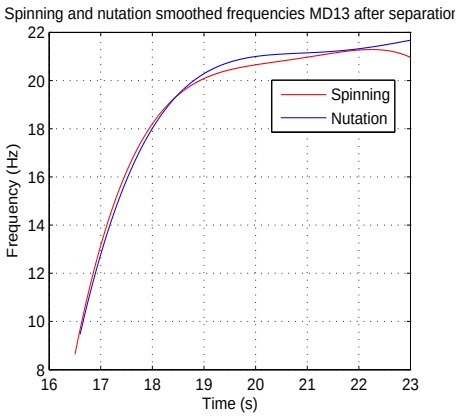

(b) Smoothed

Figure 4.11: Nutation and spinning frequency of the MD-13 after separation

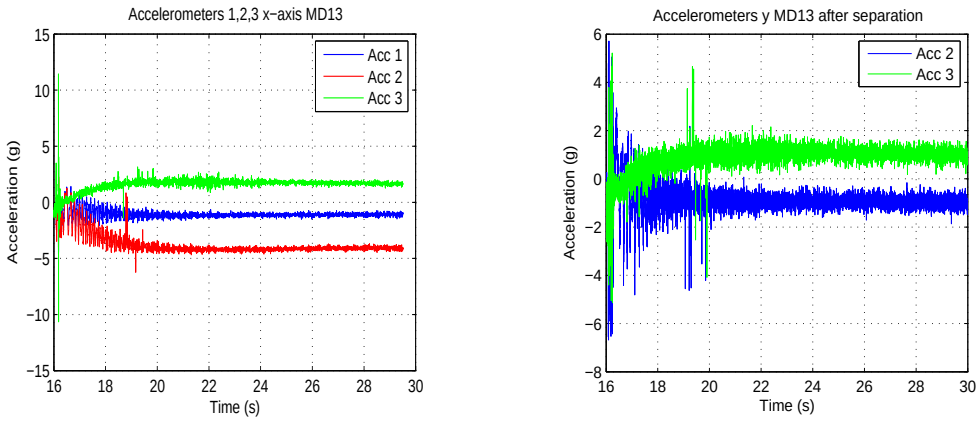

(a) x-axis (b) y-axis

Figure 4.12: Accelerometers MD-13 after separation.

for the accelerometer 1, -4.1428 g for the accelerometer 2, and 1.7545 g for the accelerometer 3. Mean values for the y-axis accelerometers are -0.9344 g for the accelerometer 2, and 1.0765 g for the accelerometer 3. With these values is possible to obtain the location of the center of gravity of the payload after separation using Equation 4.2.1

$$\frac{pos1 - CG}{mean1} = \frac{pos2 - CG}{mean2} \tag{4.2.1}$$

where *pos1*, *pos2* are the distances from the nosecone tip to the accelerometers, *mean1*,*mean2* are the mean values noted before, and CG is the position of the center of gravity from the nosecone tip. The results can be seen in Table 4.2.

Acc	*mean1*	*mean2*	*pos1*	*pos2*	CG
1x and 3x	-1.1205	1.7545	836	215	594
1x and 2x	-1.1205	-4.1428	836	998	776
2x and 3x	-4.1428	1.7545	998	215	448
2y and 3y	-0.9344	1.0765	998	215	634

Table 4.2: Calculation of the center of gravity of MD-13 during flight.

ARR determined the payload's center of gravity 625 mm away from the nosecone tip. The only results that get closer to this value are the ones obtained with the x-axis accelerometers 1 and 3, and with the y-axis accelerometers 2 and 3. Now it is necessary to include the effect of the misalignments,

which was 1.8 mm in the -y direction for the accelerometer 1 and 2.0 mm in the +x direction for the accelerometer 2. The misalignment makes the affected accelerometers to measure a component in the acceleration that they should not. Now the process is the opposite. For giving the gravitational center between the range given by the aligned accelerometers, 625±30 mm, the acceleration measured by the accelerometer 2 in the x-axis should be above -1.86 g for 625+30 mm and above -2.12 g for 625-30 mm. The more restrictive is to be above -1.86 g. Using the Equation 4.2.2 from the circular motion theory

$$\omega^2 \cdot R = a_c \tag{4.2.2}$$

where ω is the angular velocity, R is the misaligned distance, and a_c is the centripetal acceleration, it is obtained that the accelerometer can measure up to 3.55 g more, when the rocket is spinning at 21 rps.

4.2.3 Magnetometers

Phase between x and y magnetometers

The first thing to prove with the magnetometers' data is that the measured data in the x direction is 90º out of phase from the measured data in the y direction. Looking at Figure 4.13, the left green line crosses the x magnetometer's data in a maximum and the y magnetometer's data in the middle. The right green line crosses the y magnetometer's data in a minimum and the x magnetometer's in the middle. They are 90º out of phase.

Modulation of the x and y magnetometers

In Figure 4.14 is shown the effect that has the coning on the x magnetometer. The coning, represented in the z magnetometer 'modulates' the x magnetometer data, thus both frequencies can be found in the x magnetometer. The spinning frequency is obtained looking the difference between maxima and minima of the x magnetometer's data, and the coning frequency can be obtained by looking the difference between maxima and minima of the envelope. The envelope follows the same wave as the z magnetometer, as shown in the figure, with the exception that maxima from the z magnetometer will be minima in the x magnetometer's envelope, and vice versa.

Earth's magnetic field and z-magnetometer

With the data provided by ARR about the components of the Earth's magnetic field measured in each point of the trajectory, the field that should be

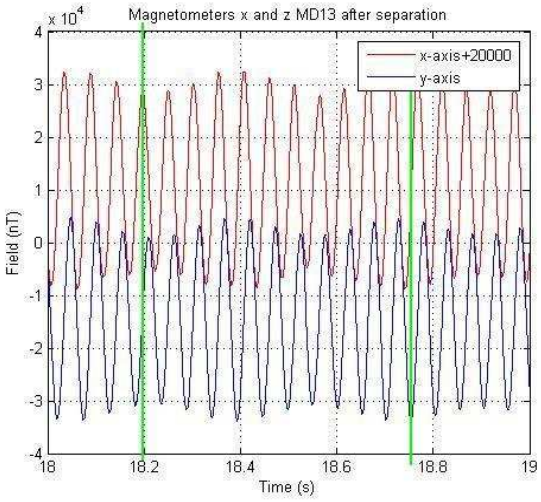

Figure 4.13: Magnetometers 90º out of phase.

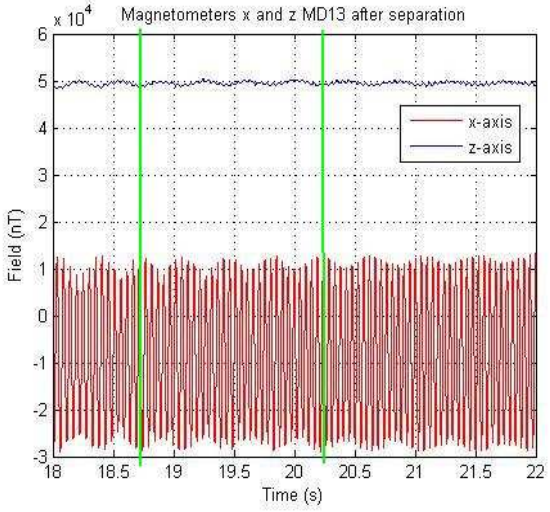

Figure 4.14: Modulation of x magnetometer's data.

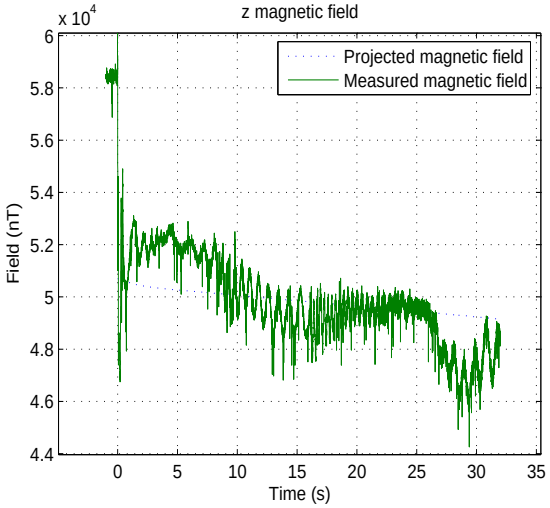

Figure 4.15: Modulation of x magnetometer's data.

measured by the rocket's z magnetometer in case only spinning existed is given in Equation 4.2.3.

$$emf_z = -B_V \cdot \sin e + \cos e \cdot (B_E \sin a + B_N \cos a) \tag{4.2.3}$$

Here B_V, B_E, and B_N are the vertical, east, and north component of the Earth's magnetic field. The elevation e , is the angle from the velocity axis to the horizontal plane. The azimuth a, is the angle measured in the horizontal plane from the north to the velocity vector's projection measured clockwise. The result is plot with the magnetometer readings in Figure 4.15

4.2.4 Coning motion

The coning motion is the most important one, not only because it provides stability but also because it can destroy completely the trajectory. Until now only qualitative study has been done on the coning motion. Now, due to the modifications of the MiniDusty payload and the motor, is necessary to know if the RS 200 SV can work well with the Mini-Dusty payload with these modifications, or if something else can be done to improve the dynamical behavior of the rocket during it's flight.

When trying to know the coning angle before separation, knowing that the coning generates a circular movement, is straight forward to think that it can be obtained with Equation 4.2.4

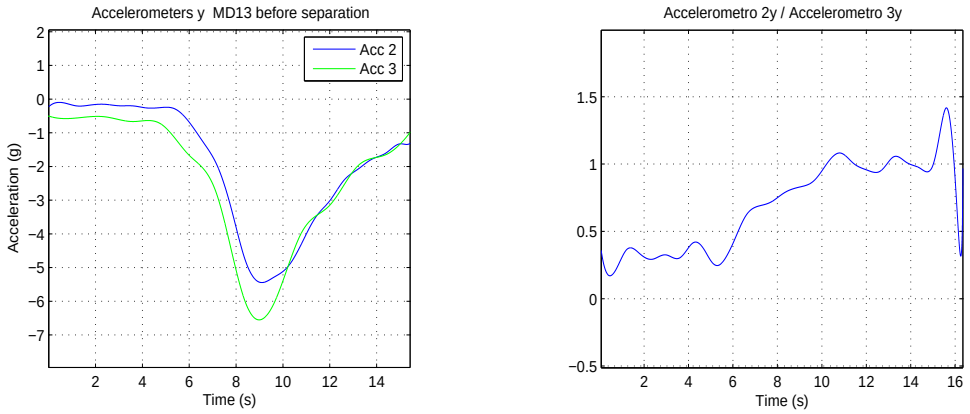

(a) Comparison (b) Division

Figure 4.16: Relation between accelerometers y-axis 2 and 3 MD13 before separation.

$$\omega^2 \cdot R \cdot \sin\gamma = (a_x \cdot \cos\gamma \cdot \cos\varphi + a_y \cdot \cos\gamma \cdot \sin\varphi + a_z \cdot \sin\gamma) \cdot g \quad (4.2.4)$$

where ω is the angular velocity of the coning motion, R is the distance from the instrumet to the rocket's center of gravity, γ is the coning angle, φ is the angle from the x-axis to the centripetal acceleration's axis. a_x, a_y, and a_z are the measured accelerations.

The distances from the accelerometers to the rocket's center of gravity are: 1929 mm for the accelerometer 1, 1767 mm for the accelerometer 2, and 2550 mm for the accelerometer 3.

But looking to the accelerometer data before separation, for example Figure 4.16, is easy to see that the relation between accelerometers 2, and 3 is not given by the relation between the distances from the accelerometers to the rocket's center of gravity, which is 0.6929. This means the motor is affecting in some way the rocket's motion, and therefore Equation 4.2.4 doesn't apply to this situation. In Figure 4.16 (a) the data are smoothed with the program A.4.3, with intervals of 0.6 s for accelerometer 2, and 1.2 s for accelerometer 3.

Looking to the accelerometer's data after separation, should be easier to know the coning angle in this part. Then find the relation between this angle with the maxima and minima from the z magnetometer, 'calibrating' in a way the z magnetometer's readings with the coning angle. Then apply this before separation.

The calculation of the coning angle after separation is based on the fact that the width of the accelerometer data is directly related with the distance

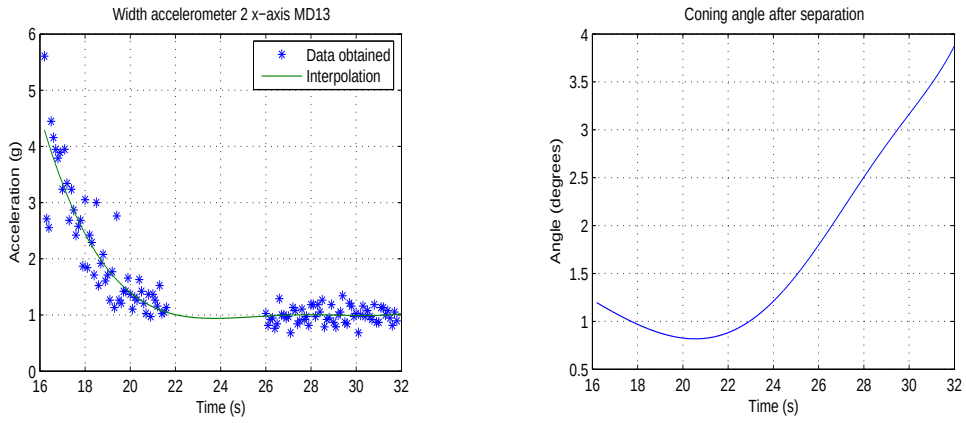

(a) Width acc 2x

(b) Division

Figure 4.17: Relation between accelerometers y-axis 2 and 3 MD13 before separation.

from the accelerometer to the velocity axis. This distance is then related with the sinus of the coning angle and the distance from the accelerometer to the payload's gravity center. The width is obtained with the program A.4.1, and the coning angle is obtained with the program A.4.2. Here is shown in Figure 4.17 (a) a graph with the width for the accelerometer, 2 y-axis in this case, and the coning angle calculated with that width in Figure4.17 (b).

The program A.4.4 smoothes first the magnetometer data with the program A.4.3, and then obtains the maxima and minima. These singularities are shown in Figure 4.18. It is necessary also to consider that the magnetic field is decreasing as we go up, so there should be made a comparision between diferences and not between absolute values between after and before separation. These values will be the the differences between the middle of the magnetometer's data and the maxima and minima. The plot of the diferences against the angle between the velocity and the magnetic field is shown in Figure 4.19.

Fitting now these values with a linear polynomial, the results are shown in Figure 4.20

The program A.4.5 smoothes first the magnetometer data before separation with the program A.4.3, and then obtains the maxima and minima. These singularities are shown in Figure 4.21. It repeats the same process as the other program, and uses the values from the linear approximation to calculate the angle. We can see the coning angle obtained with the maxima in Figure 4.22 (a), and the one obtained with the minima in Figure 4.22 (b).

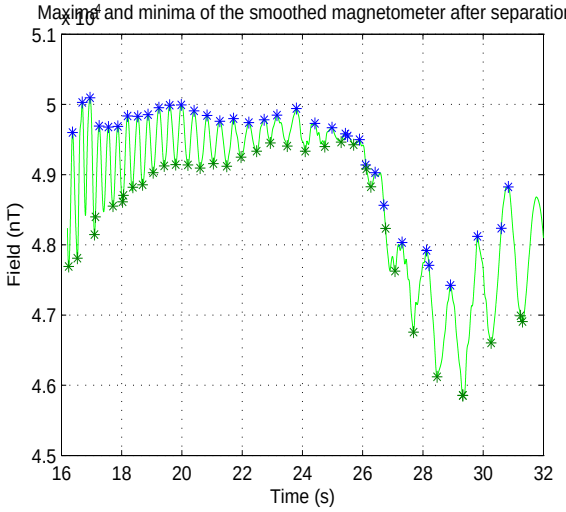

Figure 4.18: Maxima and minima in the smoothed z magnetometer's data MD13 after separation

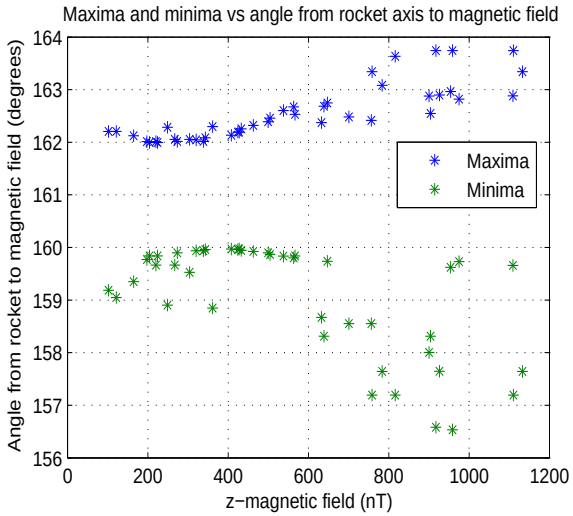

Figure 4.19: Maxima and minima in the smoothed z magnetometer's data against inclination+elevation angle, MD13 after separation

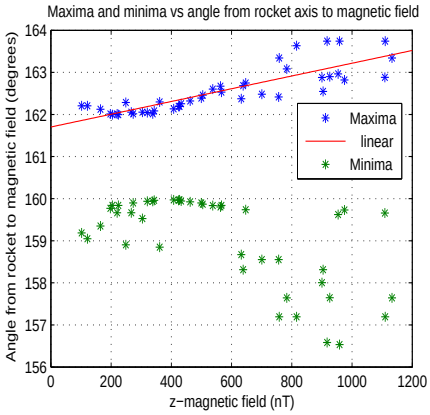

(a) Max y=0.0015148x+161.7

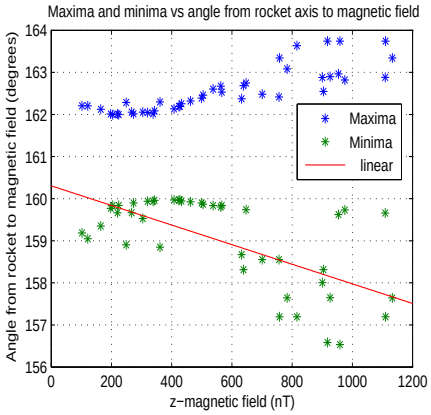

(b) Min y=-0.002329x+160.31

Figure 4.20: Linear approximation of the singularities.

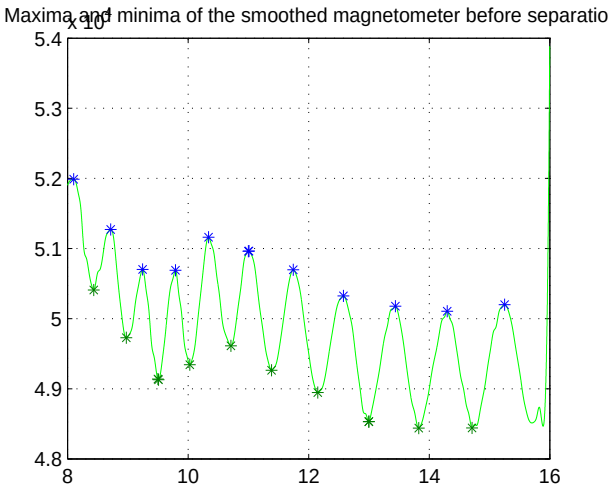

Figure 4.21: Maxima and minima in the smoothed z magnetometer's data MD13 before separation

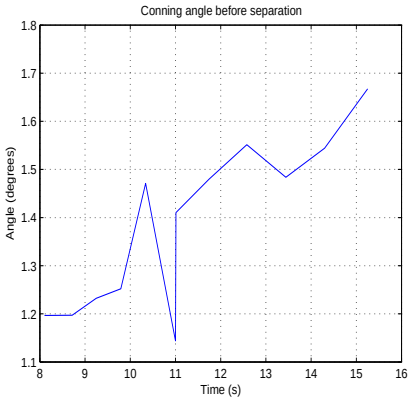

(a) Using maxima

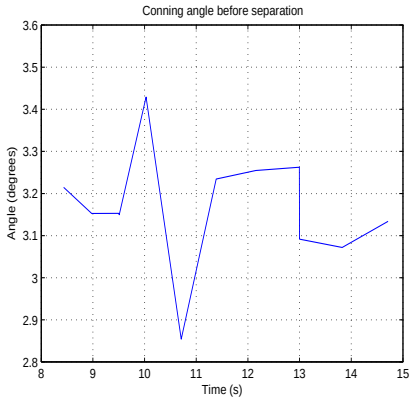

(b) Using minima

Figure 4.22: Coning angle MD13 before separation.

Chapter 5

Conclusions and further studies

In general the flight of the MD13 was at least more successful than the MD12's flight for instance. On the one hand it separated not so bad, and had a ballistic trajectory in the expected direction. On the other hand it only reached around 73 km, and this is not enough. It is not enough not only for giving time to the nosecone to turn down, it is not enough even to go through the area of interest once. This is usually due to a not very smooth separation, making the payload not to face upwards, but in this case it does not seem so.

As the results from the coning angle show, the angle was around 3 degrees when the separation took place and this is not as big as to change the trajectory of the payload. Maybe one of the reasons for not reaching enough altitude was the delayed separation. The payload should have separated at 9.3 seconds, just during the burnout. However it separated at 16.1, when the drag had braked the rocket enough to make it loose altitude.

The latter applies as far as the results from the coning angle are good. It's good also to see things from the other side, and looking after separation, the coning angle calculated with the accelerometers seemed to be increasing higher than 4 degrees. Usually the coning angle is lower after separation than before, that is why the graphs should not be taken as an absolute truth. In fact, it was a hard task to calculate this angle, and many times the situation was at an impasse, so it is necessary to be careful with this.

The motor gave near the expected maximum acceleration, only 1 or 2 g less than expected, and the use of the acceleration inside the nosecone showed that the data obtained by that accelerometer was noisier than the other's data.

The future studies will be to continue investigating the matter of the coning angle, to see if some other result can be obtained and compared with this one. There has to be a better way of finding the coning angle with only

the data from before the separation. This is something scientists really need in order to decide about more modifications of the payload of the motor, or another solution. Only qualitative research on this had been made until this thesis, and there is still more to study and to consider, as for example the same study but with the x and y magnetometers maybe can bring more light to the problem.

Appendix A

Program codes

A.1 Removing outliers

A.1.1 Remove_mag

```
function new_data=remove_mag(time,data,ini,fin,sep,mul,t,s)

% new_data=remove_mag(time,data,ini,fin,sep,mul,t,s)
% this program will remove outliers bigger than mul*std for
% magnetometer data
% ini, fin: beginning and end of the interval to remove outliers
% sep: time period subintervals of the main interval [ini,fin]
% t(1): time period for the spline interpolator before separation
% t(2): time period for the spline interpolator after separation
% s: moment of the separation
% IF NO INTERPOLATION IS WANTED t(1)=t(2)=1

% removing outliers bigger than mul*std every "sep" interval
new_data=data;
jd=find(time>=ini & time<=fin);
dev=std(new_data(jd));
a=(fin-ini)/sep;
for j=0:(a-1)
    span=find(time>=(ini+j*sep) & time<(ini+(j+1)*sep));
    datas=new_data(span);
    datas(find(abs((datas-mean(datas)))>mul*dev))=NaN;
    new_data(span)=datas;
end

% using the spline interpolator for smoothing the data with every
% t(1) point before separation and
% t(2) point after separation
mom=find(time>(s-0.1) & time<(s+0.1));
a=round(length(mom)/2)-1;       % approximate position of separation

%before separation
v=1:t(1):mom(a);
new_data(1:mom(a))=spline(time(v),new_data(v),time(1:mom(a)));
%after separation
v=mom(a):t(2):length(time);
new_data(mom(a):length(new_data))=spline(time(v),new_data(v),time(mom(a):length(time)));
```

A.1.2 Remove_acc

```
function new_data=remove_acc(time,data,ini,fin,sep,mul,t)

% new_data=remove_acc(time,data,ini,fin,sep,mul,t)
% this program will remove outliers bigger than mul*std for
% accelerometer data
% ini, fin: beginning and end of the interval to remove outliers
% sep: time period subintervals of the main interval [ini,fin]
% t time period for the spline interpolator
% IF NO INTERPOLATION IS WANTED t=1

% removing outliers bigger than mul*std every "sep" interval
new_data=data;
jd=find(time>=ini & time<=fin);
dev=std(new_data(jd));
a=(fin-ini)/sep;
for j=0:(a-1)
    span=find(time>=(ini+j*sep) & time<(ini+(j+1)*sep));
    datas=new_data(span);
    datas(find(abs((datas-mean(datas)))>mul*dev))=NaN;
    new_data(span)=datas;
end

% using the spline interpolator for smoothing the data with every
% t chosen points
v=1:t:length(time);
new_data=spline(time(v),new_data(v),time);
```

A.2 Calibration magnetometers

A.2.1 Conversion

```
function data_cal=conversion(data,i)

% data_cal=colversion(data,i)
% converts the uncalibrated values provided in nT values
% Mag x --> i=1
% Mag y --> i=2
% Mag z --> i=3

if i==1
    mx=50840*2/(3740-490);
    nx=50840-mx*3740;
    data_cal=mx*data+nx;        % nanoTeslas
elseif i==2
    my=50840*2/(3683-396);
    ny=50840-my*3683;
    data_cal=my*data+ny;        % nanoTeslas
else
    mz=50840*2/(3646-463);
    nz=50840-mz*3646;
    data_cal=mz*data+nz;        % nanoTeslas
end
```

A.3 Calculating frequencies

A.3.1 Min_max

```
function [indices,time_index_min,time_index_max,mini,maxi]=min_max(data,times)
```

```
% [indices,time_index,sing]=min_max(data,times)
% calculates the maxima and minima values of data
% time_index tells us the indices of the time moment of the singularities
% sing tells us the values of the singularities
% indices tells us how many singularities we have
% times are the indices of the data to consider

index_min=0;
index_max=0;

for i=times(1):times(length(times)) %time indices between 4s and 16s
    if (data(i-30)>data(i) & data(i-20)>data(i)& data(i-10)>data(i) &...
            data(i-5)>data(i) & data(i-4)>data(i) & data(i-3)>data(i) &...
            data(i-2)>data(i) & data(i-1)>data(i) & data(i+1)>data(i) &...
            data(i+2)>data(i) & data(i+3)>data(i) & data(i+4)>data(i) &...
            data(i+5)>data(i) & data(i+10)>data(i) & data(i+20)>data(i) &...
            data(i+30)>data(i) & data(i+40)>data(i) & data(i-40)>data(i))
        %time indices for the minima values
        time_index_min(index_min+1)=i;
        %minima
        mini(index_min+1)=data(i);
        index_min=index_min+1;
    elseif (data(i-30)<data(i) & data(i-20)<data(i) & data(i-10)<data(i) &...
            data(i-5)<data(i)  & data(i-4)<data(i) & data(i-3)<data(i) &...
            data(i-2)<data(i) & data(i-1)<data(i) & data(i+1)<data(i) &...
            data(i+2)<data(i) & data(i+3)<data(i) & data(i+4)<data(i) &...
            data(i+5)<data(i) & data(i+10)<data(i) & data(i+20)<data(i) &...
            data(i+30)<data(i) & data(i+40)<data(i) & data(i-40)<data(i))
        %time indices for the maxima values
        time_index_max(index_max+1)=i;
        %maxima
        maxi(index_max+1)=data(i);
        index_max=index_max+1;
    end
end
indices=[index_min,index_max];
```

A.3.2 Frequencies

```
function [f,m]=frequencies2(times)

%frequencies(times)
%times has the minimums (1st row) and maximums (2nd row)
%f are the frequencies in rps (Hz) that has the motion
%in each moment included in m

i=1:length(times)-1;
j=2:length(times);

%-------------USING MINIMA-----------------
diff=times(1,j)-times(1,i);
m=times(1,j);
f=1./diff;
%----------------------------------------
```

A.4 Coning angle

A.4.1 Borders

```
function [data_min,data_max,t]=borders(time,data,ini,fin,sep)

jd=find(time>=ini & time<=fin);
a=round((fin-ini)/sep);
i=1;

for j=0:(a-2)
    span=find(time>=(ini+j*sep) & time<(ini+(j+1)*sep));
    ma=max(data(span));
    mi=min(data(span));
    %m=mean(data(span));
    %d=std(data(span));
    mini(i)=mi;
    maxi(i)=ma;
    t(i)=ini+j*sep;
    i=i+1;
end
data_min=mini;
data_max=maxi;
%data_min=interp1(t,mini,time(jd),'linear');
%data_max=interp1(t,maxi,time(jd),'linear');
```

A.4.2 Coning_before

A.4.3 Media

```
function [data_med,t]=media(time,data,ini,fin,sep)

% [data_med,t]=media{time,data,ini,fin,sep}
% returns in data_med the mean of several intervals between ini and fin
% sep is the length of the intervals
% t are the moments, here, the first time of each interval

jd=find(time>=ini & time<=fin);
a=round((fin-ini)/sep);
i=1;

for j=0:(a-2)
    span=find(time>=(ini+j*sep) & time<(ini+(j+1)*sep));
    m(i)=mean(data(span));
    t(i)=ini+j*sep;
    i=i+1;
end

data_med=m;
```

A.4.4 Calibrating_after

```
function calibrating_after(time,mag,ini,fin,gamma,ie13,emf_z)

j=find(time>=ini & time<=fin);
aux=time(j);
taux=time(j);
field=emf_z(j)';
angle=ie13(j);      %inclination+elevation

%smoothing the data
[med,tmed]=media(time,mag,ini,fin,0.05);
```

```
med=spline(tmed,med,time(j));


%finding the maxima and minima of z magnetometer
jb=find(taux<=24);
a=round((fin-ini)/0.32);
clear t
i=1;
for ja=0:(a-1)
    span=find(taux>=(ini+ja*0.30) & taux<(ini+(ja+1)*0.32));
    ma(i)=max(med(span));
    b=taux(span);
    ind=find(med(span)==ma(i));
    tma(i)=b(ind);
    i=i+1;
end

i=1;
a=round((fin-ini)/0.32);
for ja=0:(a-1)
    span=find(taux>=(ini+ja*0.31) & taux<(ini+(ja+1)*0.32));
    mi(i)=da_minimo(med(span));
    b=taux(span);
    ind=find(med(span)==mi(i));
    tmi(i)=b(ind);
    i=i+1;
end

figure(1)
plot(time(j),med,'g',tma,ma,'*',tmi,mi,'*'), grid
title('Maxima and minima of the smoothed magnetometer after separation')
xlabel('Time (s)'), ylabel('Field (nT)')

%transforming the indices tma and tmi in indeces from the
%period defined by ini and fin
ama=1;
for i=1:length(tma)
    ind_ma(ama)=find(aux==tma(i));
    ama=ama+1;
end
ami=1;
for i=1:length(tmi)
    ind_mi(ami)=find(aux==tmi(i));
    ami=ami+1;
end


medio=(ma+mi)/2;
dif_ma=ma-medio;
dif_mi=medio-mi;

figure(2)
plot(dif_ma,angle(ind_ma)+gamma(ind_ma),'*',dif_mi,angle(ind_mi)-gamma(ind_mi),'*'), grid
title('Maxima and minima vs angle from rocket axis to magnetic field')
xlabel('z-magnetic field (nT)'), ylabel('Angle from rocket to magnetic field (degrees)')
legend('Maxima','Minima')
```

A.4.5 Calibrating_before

```
function calibrating_before(time,mag,ini,fin,gamma,ie13,emf_z)

j=find(time>=ini & time<=fin);

[med,tmed]=media(time,mag,ini,fin,0.045);
med=spline(tmed,med,time(j));
taux=time(j);
field=emf_z(j)';
a=round((fin-ini)/0.5);

i=1;
for ja=0:(a-2)
    span=find(taux>=(ini+ja*0.5) & taux<(ini+(ja+1)*0.5));
    ma(i)=max(med(span));
    b=taux(span);
    ind=find(med(span)==ma(i));
    tma(i)=b(ind);
    i=i+1;
end
tma(length(tma)-1)=[];
tma(9)=[];tma(11)=[];
ma(length(ma)-1)=[];
ma(9)=[];ma(11)=[];

i=1;
a=round((fin-ini)/0.5);
for ja=0:(a-2)
    span=find(taux>=(ini+ja*0.5) & taux<(ini+(ja+1)*0.5));
    mi(i)=da_minimo(med(span));
    b=taux(span);
    ind=find(med(span)==mi(i));
    tmi(i)=b(ind);
    i=i+1;
end
tmi(8)=[];tmi(12)=[];tmi(13)=[];
mi(8)=[];mi(12)=[];mi(13)=[];
figure(11)
plot(time(j),med,'g',tma,ma,'*',tmi,mi,'*'), grid
title('Maxima and minima of the smoothed magnetometer before separation')

%real indices
ama=1;
for i=1:length(tma)
    ind_ma(ama)=find(taux==tma(i));
    ama=ama+1;
end
ami=1;
for i=1:length(tmi)
    ind_mi(ami)=find(taux==tmi(i));
    ami=ami+1;
end

p_max=[0.0015148 161.7];
p_min=[-0.002329 160.31];

%dif_ma=ma-field(ind_ma);
%dif_mi=field(ind_mi)-mi;
medio=(ma+mi)/2;
dif_ma=ma-medio;
dif_mi=medio-mi;

ang_max=polyval(p_max,dif_ma);
ang_min=polyval(p_min,dif_mi);
```

```
angle=ie13(j);

figure(12)
plot(dif_ma,ang_max,'*',dif_mi,ang_min,'*'), grid

figure(13)
plot(taux(ind_ma),ang_max-angle(ind_ma)'), grid
title('Conning angle before separation')
xlabel('Time (s)'), ylabel('Angle (degrees)')
figure(14)
plot(taux(ind_mi),angle(ind_mi)'-ang_min), grid
title('Conning angle before separation')
xlabel('Time (s)'), ylabel('Angle (degrees)')
```

Bibliography

[1] F. K. Lutgens, and E. J. Tarbuck, *The Atmosphere*, Prentice Hall, 6th edition, 1995.

[2] F. de Grant, *L'œuvre de Torricelli. Science galiléenne et nouvelle géométrie*, Les Belles Lettres, 1987.

[3] A. Egeland, and E. Leer, *Professor Kr. Birkeland: His Life and Work*, IEEE Transactions on Plasma Science, vol. 4, no. 6, December, 1986.

[4] R. T. Merrill, M. W. McElhinny, and P. L. McFadden, *The magnetic field of the Earth*, International Geophysics Series, vol. 63, Academic Press, 1996.

[5] H. S. W. Massey, and R. L. F. Boyd, *The upper atmosphere*, Hutchinson of London, 1958.

[6] M. Kallenrode, *Space Physics: an introduction to plasmas and particles in the heliosphere and magnetosphere*, 2nd edition, Springer, Verlag Berlin Heidelberg, 2001.

[7] O. Havnes, *et al.*, *First detection of charged dust particles in the Earth's mesosphere*, Journal of Geophysical Research, vol. 101, no. A5, pp. 10839-10847, May 1996.

[8] M. Rapp, and F. J. Lübken, *Polar mesosphere summer echoes (PMSE): review of observations and current understanding*, Atmospheric Chemistry and Physics, vol. 4, pp. 2601-2633, 2004.

[9] Courtesy Australian Antarctic Division Commonwealth of Australia, 2006

[10] A. A. Kokhanovsky, *Microphysical and optical properties of noctilucent clouds*, Earth-Science Reviews, vol. 71, pp. 127-146, 2005.

[11] O. Havnes, C. La Hoz, and L. I. Næsheim, *First observations of the PMSE overshoot effect and its use for investigating the conditions in the summer mesosphere*, Geophysical Research Letters, vol. 30, no. 23, 2003.

[12] E. M. Marconi, *What is a sounding rocket?*, Research Aircraft, NASA, 2004.

[13] Andøya Rocket Range, *http://www.rocketrange.no/arr/index.html*. Last online query June,2007.

[14] Arctic Lidar Observatory for Middle Atmosphere Research, *http://alomar.rocketrange.no/*. Last online query June, 2007.

[15] EISCAT, *https://e7.eiscat.se/groups/Documentation/BasicInfo/locations.html*. Last online query June, 2007

[16] J. M. Krause, *Rocket systems for meteorological and upper atmospheric soundings*, 13th ESA Symposium on Rocket and Balloon Programmes and Related Research, Lillehammer, Norway, ESA SP-370, 1995.

[17] Forces acting on a rocket, *http://exploration.grc.nasa.gov/education/rocket/rktfor.html*, National Aeronautics and Space Administration, NASA. Last online query June, 2007.

[18] National Aeronautics and Space Administration, NASA, *Sounding rocket program handbook*, June 1, 1999.

[19] Jan-Erik Rnningen, *Rocket aerodynamics and stability - an introduction*, Speech given in Andøya Rocket Range, November, 2006.

[20] The World Magnetic Model, *http://www.ngdc.noaa.gov/seg/WMM/DoDWMM.shtml*, National Geophysical Data Center. Last online query June, 2007.

[21] O. Havnes, E. Haugen, T. Tønnesen, and I. Nyheim, *Flight requirements plan for Mini-Dusty 6,7, and 8*, Andøya Rocket Range, Andenes, July 1st, 1999.

[22] S. V. Olsen, and D. Noteborn, *Manual for preparing a Mini-Dusty payload*, ver. 1.0.

[23] Cortesy of Sveinung V. Olsen, University of Tromsø, Norway.

[24] P. Yeh, and C. Gu, *Optics of Liquid Crystal Displays*, Wiley, pp. 75-86, 1999.

[25] Honeywell data sheet, *1- and 2- axis magnetic sensors. HMC1001 / HMC1002.*

[26] Analog Devices data sheet, ±5 *g to* ±50 *g, low noise, low power, single/dual axis i*MEMS® *accelerometers.*

[27] O. Havnes, S. V. Olsen, E. Haugen, T. Kristiansen, P. Dragøy, *Flight requirements plan for Mini-Dusty / RH200 SV Campaign*, ARR-P-337, Andøya Rocket Range, Andenes, February 15th, 2007.

[28] The MathWorks Website, *http://www.mathworks.co.uk/index.html?ref=logo.* Last online query June, 2007.